REPORT DOCUMENTATION PAGE

Form Approved OMB NO. 0704-0188

1. REPORT DATE (DD-MM-YYYY)	2. REPORT TYPE	3. DATES COVERED (From - To)
07-11-2014	Final Report	9-May-2011 - 8-Aug-2014

4. TITLE AND SUBTITLE
Final Report: Optical Spectroscopy of Hybrid Semiconductor Quantum Dots and Metal Nanoparticles

5a. CONTRACT NUMBER
W911NF-11-1-0177

5b. GRANT NUMBER

5c. PROGRAM ELEMENT NUMBER
206022

6. AUTHORS
Jaetae Seo

5d. PROJECT NUMBER

5e. TASK NUMBER

5f. WORK UNIT NUMBER

7. PERFORMING ORGANIZATION NAMES AND ADDRESSES
Hampton University
100 E. Queen Street

Hampton, VA 23668 -0108

8. PERFORMING ORGANIZATION REPORT NUMBER

9. SPONSORING/MONITORING AGENCY NAME(S) AND ADDRESS (ES)
U.S. Army Research Office
P.O. Box 12211
Research Triangle Park, NC 27709-2211

10. SPONSOR/MONITOR'S ACRONYM(S)
ARO

11. SPONSOR/MONITOR'S REPORT NUMBER(S)
58943-EL-REP.14

12. DISTRIBUTION AVAILIBILITY STATEMENT
Approved for Public Release; Distribution Unlimited

13. SUPPLEMENTARY NOTES
The views, opinions and/or findings contained in this report are those of the author(s) and should not contrued as an official Department of the Army position, policy or decision, unless so designated by other documentation.

14. ABSTRACT
Optical studies of semiconductor quantum dots (SQDs), metal nanoparticles (MNPs), and their hybrid nanomaterials are great interests for the Department of Defense's (DoD) photonic applications. Our research focused on developing and characterizing advanced optical nanomaterials of hybrid plasmon-coupled semiconductor quantum dots, II-VI semiconductor QDs, and I-III-VI2 semiconductor nanocrystals (SNCs). The coupling distances between the mono-layers of Au nanoparticles were controlled by PMMA plasma etching. The time-resolved spectroscopy of plasmon-coupled II-VI semiconductor QDs revealed a strong shortening of the

15. SUBJECT TERMS
Optical Spectroscopy of Semiconductor Nanocrystals

16. SECURITY CLASSIFICATION OF:			17. LIMITATION OF ABSTRACT	15. NUMBER OF PAGES	19a. NAME OF RESPONSIBLE PERSON
a. REPORT	b. ABSTRACT	c. THIS PAGE			Jaetae Seo
UU	UU	UU	UU		19b. TELEPHONE NUMBER 757-727-5149

Report Title

Final Report: Optical Spectroscopy of Hybrid Semiconductor Quantum Dots and Metal Nanoparticles

ABSTRACT

Optical studies of semiconductor quantum dots (SQDs), metal nanoparticles (MNPs), and their hybrid nanomaterials are great interests for the Department of Defense's (DoD) photonic applications. Our research focused on developing and characterizing advanced optical nanomaterials of hybrid plasmon-coupled semiconductor quantum dots, II-VI semiconductor QDs, and I-III-VI2 semiconductor nanocrystals (SNCs). The coupling distances between the mono-layers of Au nanoparticles were controlled by PMMA plasma etching. The time-resolved spectroscopy of plasmon-coupled II-VI semiconductor QDs revealed a strong shortening of the longest lifetime and ~9-fold PL enhancement. For the I-III-VI2 semiconductor nanocrystals, both time-resolved and temperature-dependent photoluminescence spectroscopy revealed their optical properties with spectral, temporal, and thermal characteristics which were closely linked to surface related recombination, and shallow or deep defect-related donor-acceptor transitions. The good spectral coupling between the PL from CIS/ZnS with a broad spectral width and the InGaN diode excitation leads to the realization of hybrid white LEDs.

Enter List of papers submitted or published that acknowledge ARO support from the start of the project to the date of this printing. List the papers, including journal references, in the following categories:

(a) Papers published in peer-reviewed journals (N/A for none)

Received		Paper
08/18/2012	1.00	Jaetae Seo, Rafal Fudala, Wan-Joong Kim, Ryan Rich, Bagher Tabibi, Hyoyeong Cho, Zygmunt Gryczynski, Ignacy Gryczynski, William Yu. Hybrid optical materials of plasmon-coupled CdSe/ZnS coreshells for photonic applications, Optical Materials Express, (07 2012): 1026. doi:
08/18/2012	4.00	Maria Veronica Rigo, Jaetae Seo. Probing Plasmon Polarization-Mediated Photoluminescence Enhancement on Metal-Semiconductor Hybrid Optical Nanostructures, Chemical Physics Letters , (10 2011): 190. doi:
08/18/2012	5.00	Maria Veronica Rigo, Jaetae Seo, Wan-Joong Kim, SungSoo Jung. Plasmon Coupling of R6G-linked Metal Nanoparticle Assemblies for Surface-enhanced Raman Spectroscopy, Vibrational Spectroscopy , (11 2011): 315. doi:
08/21/2012	6.00	Jaetae Seo, Roopchan Ramdon, Sanghee Kim, Hyeon-Bong Pyo, Kyuho Song, Byoung Hun Kang. Solid-Phase Immunoassay of Polystyrene-Encapsulated Semiconductor Coreshells for Cardiac Marker Detection, Journal of Nanomaterials, (01 2012): 693575. doi:
11/07/2014	11.00	Quinton Rice, Sangram Raut, Rahul Chib, Zygmunt Gryczynski, Ignacy Gryczynski, Wenjin Zhang, Xinhua Zhong, Mahmoud Abdel-Fattah, Bagher Tabibi, Jaetae Seo. Fractional Contributions of Defect-originated Photoluminescence from CuInS2/ZnS Coreshells for Hybrid White LEDs, Journal of Nanomaterials, (10 2014): 979875. doi:
TOTAL:	**5**	

Number of Papers published in peer-reviewed journals:

(b) Papers published in non-peer-reviewed journals (N/A for none)

Received		Paper
08/18/2012	2.00	Bo Zou, William W. Yu, Jaetae Seo, Ting Zhu, Michael Z. Hu. Nanocrystals-Related Synthesis, Assembly, and Energy Applications 2012, Journal of Nanomaterials, (02 2012): 820439. doi:
11/07/2014	13.00	SaaraA.Khan, GenniferT.Smith, Felix Jaetae Seo, Audrey K.Ellerbee. Label-free and non-contact optical biosensing of glucose with quantum dots, Biosensors and Bioelectronics64(2015)30–35, (02 2015): 30. doi:
TOTAL:		**2**

Number of Papers published in non peer-reviewed journals:

(c) Presentations

Following this instruction "Please be sure to submit all papers to ARO separately", all abstracts will be submitted separately.

Conference Presentations:

7. Quinton Rice, Sangram Raut, Rahul Chib, Zygmunt Gryczynski, Ignacy Gryczynski, Wenjin Zhang, Xinhua Zhong, Mahmoud Abdel-Fattah, Bagher Tabibi, and Jaetae Seo, "Plasmon-coupled CuInS2/ZnS core-shells for developing hybrid white LEDs," SPIE Photonics West 2015, Feb 7-12, Moscone Center, San Francisco, CA. (Paper No.: OE117-32; Tracking No.: PW15O-OE117-32, Invited to Oral Presentation).
8. Anderson Hayes, Quinton Rice, Wan-Joong Kim, Sungsoo Jung, and Jaetae Seo, "Colorimetric Flocculation and Vibration Frequency Modification of Nicotine under Plasmonic Mode," The 12th International Conference on Nano Science and Nano Technology, November 6-7, 2014, Mokpo, South Korea.
9. Quinton Rice, Anderson Hayes, Andrew Wang, William Yu, Wan-Joong Kim, Sungsoo Jung, and Jaetae Seo, "Plasmon-Coupled CdSe Quantum Dots for Hybrid Light Emitting Devices," The 12th International Conference on Nano Science and Nano Technology, November 6-7, 2014, Mokpo, South Korea.
10. Anderson Hayes, Wan-Joong Kim, Jaetae Seo, "Colorimetric Flocculation of Intraband Transitions and Raman Frequency Changes in BioChemical Sensing Applications," 2014 NanoTechnology for Defense Conference, November 17-20, 2014, Chantilly, VA, U.S.A.
11. Quinton Rice, Roopchan Ramdon, Maria Veronica Rigo, Rafal Fudala, Wan-Joong Kim, Ryan Rich, Bagher Tabibi, Hyoyeong Cho, Zygmunt Gryczynski, Ignacy Gryczynski, Mahmoud Abdel-Fattah, William Yu, and Jaetae Seo, "Purcell Enhancement of Plasmon-coupled Semiconductor QDs for Photonic Applications," 2014 NanoTechnology for Defense Conference, November 17-20, 2014, Chantilly, VA, U. S.A.
12. Quinton Rice, Anderson Hayes, Sangram Raut, Mahmoud Abdel-Fattah, Ignacy Gryczynski, Zygmunt Gryczynski, Wenjin Zhang, Xinhua Zhong, Young-Kuk Kim, Bagher Tabibi, and Jaetae Seo, "Time-resolved Photoluminescence of Plasmon-coupled CuInS2 with ZnS," ICANM2014, International Conference & Exhibition on Advanced & Nano Materials, August 11-13, Calgary, Alberta, Canada.
13. Anderson Hayes, Quinton Rice, Mahmoud Abdel-Fattah, Min Namkung, Wan-Joong Kim, Sungsoo Jung, Bagher Tabibi, and Jaetae Seo, "Colorimetric Analysis and Spectral Coupling of SERS for Biomedical Sensing," ICANM2014, International Conference & Exhibition on Advanced & Nano Materials, August 11-13, Calgary, Alberta, Canada.
14. Quinton Rice, Sangram Raut, Ignacy Gryczynski, Zygmunt Gryczynski, Wenjin Zhang, Xinhua Zhong, Young-Kuk Kim, Bagher Tabibi, and Jaetae Seo, "Optical Properties of CuInS2 QDs with ZnS Coreshells and Alloys for Developing Hybrid LEDs," International Conference on Superlattices, Nanostructures and Nanodevices, Savannah, Georgia, August 3-8, 2014.
15. Quinton Rice, Sangram Raut, Wan-Joong Kim, Ryan Rich, Rafal Fudala, Mahmoud Abdel-Fattah, Bagher Tabibi, Ignacy Gryczynski, Zygmunt Gryczynski, Sungsoo Jung, and Jaetae Seo, "Temporal Distributions of Optical Energy Transitions and Photoluminescence Quenching in CuInS2 with ZnS Capping and Alloy," 45th Annual Meeting of the APS Division of Atomic, Molecular and Optical Physics, Madison, WI, June 2-6, 2014.
16. Quinton Rice, Maria Veronica Rigo, Rafal Fudala, Hyoyeong Cho, Wan-Joong Kim, Ryan Rich, Bagher Tabibi, Zygmunt Gryczynski, Ignacy Gryczynski, William Yu, and Jaetae Seo, "Plasmon and Exciton Coupling and Purcell Enhancement," 45th Annual Meeting of the APS Division of Atomic, Molecular and Optical Physics, Madison, WI, June 2-6, 2014.
17. Anderson Hayes, Quinton Rice, Mahmoud Abdel-Fattah, Wan-Joong Kim, Sungsoo Jung, Bagher Tabibi, and Jaetae Seo, "Time-resolved Colorimetric Flocculation and Surface-enhanced Raman Scattering of Molecule-linked Plasmonic Nanoparticles," The 92nd Annual Meeting of Virginia Academy of Science, Virginia Commonwealth University, May 14-16, 2014.
18. Quinton Rice, Sangram Raut, Ignacy Gryczynski, Zygmunt Gryczynski, Bagher Tabibi, and Jaetae Seo, "Temperature- and Time-resolved Spectroscopy of CuInS2 Semiconductor Nanocrystals with ZnS Capping," The 92nd Annual Meeting of Virginia Academy of Science, Virginia Commonwealth University, May 14-16, 2014.
19. Quinton Rice, Roopchan Ramdon, Maria Veronica Rigo, Rafal Fudala, Wan-Joong Kim, Ryan Rich, Bagher Tabibi, Hyoyeong Cho, Zygmunt Gryczynski, Ignacy Gryczynski, Mahmoud Abdel-Fattah, William Yu, and Jaetae Seo, "Plasmon-coupled Exciton Photoluminescence with Purcell Enhancement," Nanotechnology for Defense Conference, November 4-7, 2013, Tucson, Arizona.
20. Quinn Hailes, Quinton Rice, Anderson Hayes, Mahmoud Abdel-Fattah, Sangram Raut, Ryan Rich, Rafal Fudala, Ignacy Gryczynski, Zygmunt Gryczynski, Wan-Joong Kim, Sungsoo Jung, Ryo Hyun, Yu Zhang, Chuang Xie, Bagher Tabibi, William Yu, and Jaetae Seo, "Optical Properties of CuInS2 CuInS2/ZnS and ZnCuInS2 Semiconductor Nanocrystals," XXII International Materials Research Congress, August 11 - 15, 2013, Cancun, Mexico.
21. Anderson Hayes, Quinton Rice, Maria Veronica Rigo, Mahmoud Abdel-Fattah, Sainath Babu, Michelle Claville, Min Namkung, Wan-Joong Kim, Sungsoo Jung, Bagher Tabibi, and Jaetae Seo, "Spectral Coupling of Molecule-linked Au Nanoparticles for Surface-Enhanced Raman Scattering," XXII International Materials Research Congress, August 11 - 15, 2013, Cancun, Mexico.
22. M. Namkung and Jaetae Seo, "Surface-enhanced Raman Spectroscopy for Astrobiology Exploration on Mars," International Workshop on Instrumentation for Planetary Missions (IPM-2012), Greenbelt, Maryland, Oct. 10-12, 2012.

Number of Presentations: 16.00

Non Peer-Reviewed Conference Proceeding publications (other than abstracts):

Received	Paper

TOTAL:

Number of Non Peer-Reviewed Conference Proceeding publications (other than abstracts):

Peer-Reviewed Conference Proceeding publications (other than abstracts):

Received	Paper

TOTAL:

Number of Peer-Reviewed Conference Proceeding publications (other than abstracts):

(d) Manuscripts

Received	Paper	
08/30/2013	7.00	Ignacy Gryczynski, Zygmunt Gryczynski, Wan-Joong Kim, Sungsoo Jung, Ruh Hyun , Jaetae Seo , Sangram Raut, Mahmoud Abdel-Fattah, Quinton Rice, Bagher Tabibi, Ryan Rich, Rafal Fudala. Time-resolved and temperature-dependent photoluminescence of ternary and quaternary nanocrystals of CuInS2 with ZnS capping and cation exchange, Journal of Applied Physics (06 2013)

TOTAL: **1**

Number of Manuscripts:

Books

Received Book

TOTAL:

Received Book Chapter

TOTAL:

Patents Submitted

Patents Awarded

Awards

Honors and Awards

1. Dr. Jaetae Seo received a continuing grant increment from the National Science Foundation. The award for continuing grant increment is $3,000,000 from September 01, 2011 to August 31, 2014. The project is entitled “Advanced Center for Laser Science and Spectroscopy,” with total budget $5,000,000 from September 01, 2011 to August 31, 2016. Dr. Seo is serving as a PI and Program Director.
2. Dr. Jaetae Seo is served as an Editor-in-Chief for the Journal of Photonics and Optoelectronics, and serving as an Editorial Board of Photonics and Optoelectronics, Editorial Board of The Open Spectroscopy Journal, Editorial Board for Optics and Photonics Journal, and Editorial Advisory Board of the Open Applied Physics Journal.
3. Dr. Jaetae Seo invited to the Ginzton Laboratory, Stanford University, to study optical properties of semiconductor quantum dots in 2013.
4. Mr. Quinton Rice attended the 92nd Annual Meeting of the Virginia Academy of Science in Richmond, Virginia on May 14th through May 16th 2014 at Virginia Commonwealth University. He presented on “Temperature- and time-resolved spectroscopy of CuInS2 semiconductor nanocrystals with ZnS capping” in the Astronomy, Math, and Physics with Material Science Section with Thomas C. Mosca III presiding as Chair. Mr. Rice was awarded 1st place in the oral presentation competition for Best Student Paper Presentation.
5. Mr. Anderson Hayes is served as the District Council Representative for Zone 4 of the National Society of Physics Students.
6. Ms. Rahda Venkatesan, Junior, Grafton High School and Governor's School, presented her research results at the 62nd Tidewater Science Fair Competition, and received 1st place award in Materials and Bio-engineering category. Her presentation title was “Surface-Enhanced Raman Scattering for Quinine-linked Gold Nanoparticles”. Tidewater Regional Science and Engineering Fair was held at Old Dominion University, Norfolk Virginia on March 16, 2013. Ms. Radha Venkatesan also participated in the Virginia State Science & Engineering Fair on April 5-6, 2013 at Virginia Military Institute, Lexington, VA. The Virginia State Science Fair was affiliated with the International Science and Engineering Fair. High school students from across the state competed within 13 categories. The grand prize winner was proceeded to participate in the Intel International Science and Engineering Fair. At the State Science Fair, Ms. Venkatesan received two special awards for the project. One was from SAIC for Applied Sciences. The other one was the Yale Science and Engineering Award presented by Yale University for the Most Outstanding 11th grade Exhibit Overall from the categories of Computer Science, Engineering, Physics or Chemistry. Recently, she was admitted to the physics program at the University of Richmond with the Presidential Scholarship $60,000, and is chosen to be a Richmond Science Scholar with Robins Science Scholar designation with $229,880.

Graduate Students

NAME	PERCENT_SUPPORTED	Discipline
Anderson Hayes	0.17	
Quinton Rice	0.22	
Ashely Jackson	0.55	
Roopchan Ramdon	0.61	
Yuriy Pipiskiy	0.08	
FTE Equivalent:	**1.63**	
Total Number:	**5**	

Names of Post Doctorates

NAME	PERCENT_SUPPORTED
Mahmoud Abdel-Fattah	0.14
FTE Equivalent:	**0.14**
Total Number:	**1**

Names of Faculty Supported

NAME	PERCENT_SUPPORTED	National Academy Member
Jaetae Seo	0.44	
FTE Equivalent:	**0.44**	
Total Number:	**1**	

Names of Under Graduate students supported

NAME	PERCENT_SUPPORTED	Discipline
Quinton Rice	0.00	B.S.
Anderson Hayes	0.00	B.S.
Quinn Hailes	0.00	B.S.
FTE Equivalent:	**0.00**	
Total Number:	**3**	

Student Metrics

This section only applies to graduating undergraduates supported by this agreement in this reporting period

The number of undergraduates funded by this agreement who graduated during this period: 3.00

The number of undergraduates funded by this agreement who graduated during this period with a degree in science, mathematics, engineering, or technology fields:..... 3.00

The number of undergraduates funded by your agreement who graduated during this period and will continue to pursue a graduate or Ph.D. degree in science, mathematics, engineering, or technology fields:..... 3.00

Number of graduating undergraduates who achieved a 3.5 GPA to 4.0 (4.0 max scale):..... 0.00

Number of graduating undergraduates funded by a DoD funded Center of Excellence grant for Education, Research and Engineering:..... 0.00

The number of undergraduates funded by your agreement who graduated during this period and intend to work for the Department of Defense 0.00

The number of undergraduates funded by your agreement who graduated during this period and will receive scholarships or fellowships for further studies in science, mathematics, engineering or technology fields:..... 0.00

Names of Personnel receiving masters degrees

NAME
Roopchan Ramdon
Total Number: 1

Names of personnel receiving PHDs

NAME
Total Number:

Names of other research staff

NAME	PERCENT_SUPPORTED
FTE Equivalent:	
Total Number:	

Sub Contractors (DD882)

Inventions (DD882)

Scientific Progress

Please find the attachment.

Technology Transfer

None

Scientific Progress and Accomplishments

1. Examples of Specific research activities and findings:

Hybrid optical materials of plasmon-coupled CdSe/ZnS coreshells for photonic applications

Hybrid optical materials consisting of semiconductor quantum dots (SQDs) and plasmonic metal nanoparticles are of great interest for photonic and biomedical applications.[1] The SQDs of cadmium and lead chalcogenide (Te, Se, and S) have been extensively studied because of their high internal quantum efficiencies and wide optical tunability of absorption and emission spectra in the visible and near-infrared spectral region with quantum confinements at sizes near their Bohr radii.[2] Although the colloidal SQDs in solution exhibit high internal quantum efficiencies,[3] their luminescence efficiencies considerably drop when the SQDs are casted into the thin films for photonic applications,[4] as shown in figure 1. However, the internal quantum efficiency of SQDs in the proximity of plasmonic nanoparticles significantly changes when excitons and plasmons coherently interact via the Coulomb force. The changes in PL enhancement and quenching are closely related to the coupling distance. Therefore large changes in the optical properties of SQDs in the proximity of plasmonic nanoparticles are anticipated to be achieved by controlling the coupling distance.[5]

The hybrid nanomaterials of Au-PMMA-CdSe/ZnS were assembled on quartz slides with a size of 10×10 mm^2. The quartz surface was hydroxylated using an oxygen plasma (Plasma System V15-G, Plasma Finish) with operation conditions of 30 Pa, oxygen 100 ml/min, and 100 watts for 300 sec. The hydroxylated quartz was silanized in ethanol containing 1 wt. % 3-aminopropyltriethoxysilane (APTES, Sigma-Aldrich, CAS#: 919-30-2) in order to form the amino (NH_2) functional group on the surface of the hydroxylated quartz. The amino functionalized quartz plate was washed with ethanol, and dried with nitrogen gas. Finally, the dried quartz was baked at 120 ^oC for 15 minutes. The amine reactivated-quartz was spotted with the high concentration Au nanoparticles for 12 hours at room temperature, and washed with de-ionized water, and dried with nitrogen gas. The schematic procedure of hydroxylation, amino functionalization, and Au nanoparticle deposition is depicted in the figure 2(a). The Au nanoparticle deposition images on the quartz plate were analyzed with an atomic force microscope (AFM, Agilent, 5500AFM). The image indicated that the Au nanoparticles were well mounted on the quartz plate without multi-layers or aggregations.

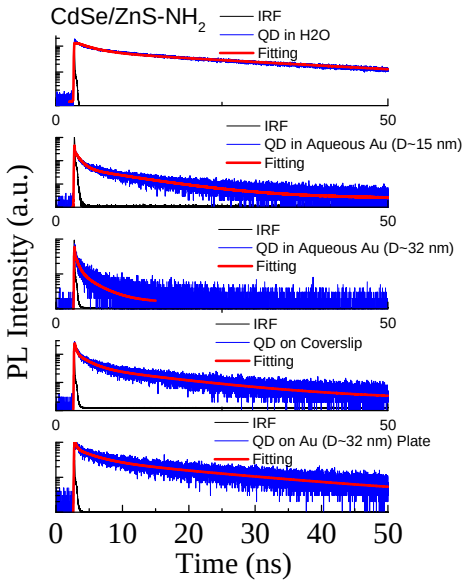

Figure 1. Fluorescence lifetime dynamics of NH_2-functionalized CdSe/ZnS coreshells in water, on the surface of Au nanoparticles, and on the cover glass. The NH_2 functional group has a strong affinity with Au nanoparticles.

For preparing a spacer with thickness from ~1 to ~50 nm between CdSe/ZnS SQDs and Au NPs, poly(methyl methacrylate) (PMMA, C2 950k) with a volume of 0.1 ml was casted on the Au NPs-attached quartz plate using a spin coater (SP-1, SPIN Programmer, ABLE Co.) at 5000 rpm for 30 sec. The PMMA/Au/quartz plate was subsequently baked at 120 °C for 2 min. The thickness of the PMMA spacer between Au NPs and CdSe SQDs was controlled by oxygen plasma etching with operation conditions of 30 Pa, oxygen 100 ml/min, and 100 watts for 7 min, 12 min, 17 min, 20 min, 25 min, 27 min, and 30 min, respectively. For the thickness of PMMA spacer from ~50 to ~100 nm between CdSe/ZnS SQDs and Au NPs, PMMA with a volume of 0.1 ml was casted on the Au-attached quartz plate using the same spin coater at 3500 rpm for 30 sec, and then the plate was baked at 120 °C for 2 min. The thickness of PMMA was controlled by plasma etching for 7 min, 12min, 17 min, and 22 min, respectively. The plasma etching has been used to prepare a uniform morphology and stable surface [23, 24], and it provided control of the PMMA thickness to within ~1 nm. In the plasma etching process, neutral and radical oxygen is produced by the reactions of $O_2 + O^+ \rightarrow O_2^+ + O$ and $O_2^+ + e^- \rightarrow O + O$. The radical oxygen attracts a hydrogen atom, and creates an OH and a hydrocarbon chain. The oxygen species breaks the polymer hydrocarbon chain into small pieces. In this procedure, the plasma etching simply bombards surfaces of PMMA with energetic particles that knock off surface particles.

After surface treatment of PMMA with oxygen plasma, casein (0.1 ml of 1% protein) in solution of 1xPBS (phosphate buffered saline) was spin-coated at 3,500 rpm for 30 sec on the PMMA/Au/quartz plate to reform the hydrophobic surface of PMMA to hydrophilic. Then, the

CdSe/ZnS-COOH was properly bound on the hydrophilic PMMA. For developing hybrid plasmon-coupled SQDs, CdSe/ZnS SQDs with a volume of 0.1 ml of ~10 μM was casted on the plate at 3,500 rpm for 30 sec. The final layer of PMMA with a volume of 0.01 ml was coated to protect the SQDs from ambient environments. Also, both a PMMA/SQDs/PMMA/quartz plate without Au nanoparticles and a PMMA/Au/quartz plate without SQDs were prepared for comparison purposes.

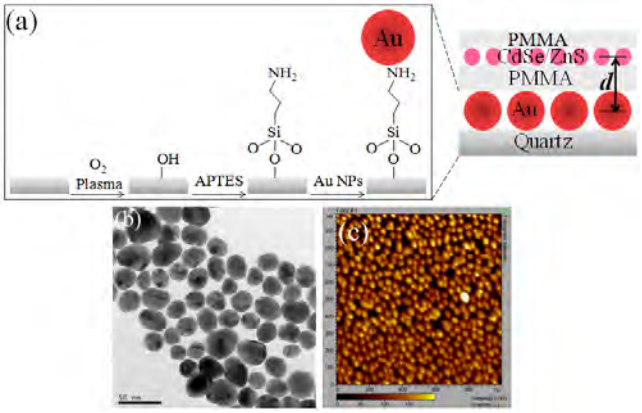

Figure 2. (a) Schematic procedure of hydroxylation, amino functionalization, and Au deposition, (b) TEM image of Au nanoparticles, and (c) AFM image (1 μm × 1 μm) of Au nanoparticle depositions on quartz plate.

The resulting hybrid nanostructures of plasmon-coupled SQDs were analyzed with a field-emission scanning electron microscope (FE-SEM, FEI, Sirion) as shown in figure 3. The lateral images of PMMA/Au/quartz plate were produced by the FE-SEM with operation conditions of 10.0 KV as shown in figure 3 (a) and (b). The samples for lateral view analyses with FE-SEM were coated by a platinum (Pt) layer with a thickness of less than ~10 nm to create clear images by reducing charge activities on the quartz plate due to the energetic electrons. The image of figure 3 (a) displays the lateral view of a PMMA/Au/quartz plate at a slight angle without a sample cut. The image of the top surface in the figure 3 (a) displays Au nanoparticle distribution under the PMMA film. The image of figure 3 (b) exhibits a lateral view of the PMMA/Au/quartz plate after it was cut with a diamond knife (Ogura Jewel Industry Co., D-Point Pen). The rear side of sample (quartz) was scratched with the diamond knife, and cut in a uni-direction with ambient weak mechanical force. The image displays a single layer of Au nanoparticles with uniform and regular distribution through NH_2 functional group on the quartz plate.

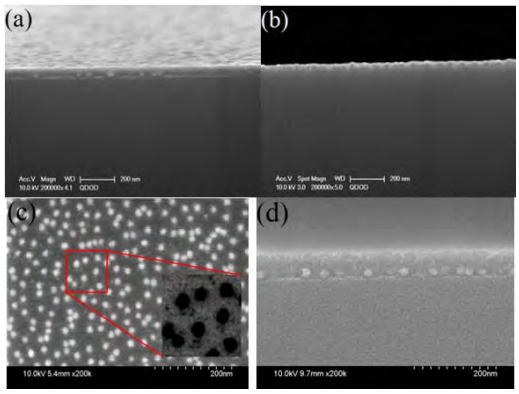

Figure 3. SEM images of lateral views of PMMA/Au on a quartz plate (a) as it was prepared, and (b) after it was cut with a diamond knife. SEM images on (c) the top, and (d) the lateral views of QD/PMMA/Au on a quartz plate. The inset in fig. (c) was an inversion of bright and dark image.

The top view of QD/PMMA/Au/quartz plate was presented in figure 3 (c). The image was also analyzed using a field-emission scanning electron microscope (FE-SEM, FEI, Sirion) with operation conditions of 10 KV. It was interesting to see the Au nanoparticles through the PMMA with a contrast image technique of FE-SEM. Even though the image did not display the complete morphology of Au nanoparticles, the number density of nanoparticles was able to be estimated. The number density of Au nanoparticles (D~32 nm) was estimated to be ~9.18×10^{-4} nm^{-2}, which indicated ~9 particles in the area of 100 ×100 nm^2. The inset of figure 3 (c) is a picture reformation with -35% brightness and 35% contrast after the dark and bright images of figure 3 (c) were inverted. The inset image in figure 3(c) displays Au nanoparticles and SQDs with large black dots and small dots, respectively. The number density of SQDs was roughly estimated to be ~3.7×10^{-3} nm^{-2} by the inverted image of the figure 3 (c).

To analyze the coupling distance from the layer of Au nanoparticles on the quartz plate to the layer SQDs on the surface of PMMA, the lateral view of QD/PMMA/Au/quartz plate with pt coating was also characterized with the FE-SEM (FEI) with operation conditions of 10 KV. The lateral views for estimating the coupling distance were taken from the sample as it was prepared without an additional cut. A typical image for estimating coupling distance from the center of Au layer to the center of QD layer is shown in figure 3 (d). The layer distance was calculated to be ~45.5 nm after the radii of Au nanoparticles and SQDs were subtracted from the thickness between the top of the quartz and the top of the PMMA. The different sample thicknesses were prepared in various casting and plasma etching conditions which were described above for microscopic and optical analyses.

Figure 4 shows the normalized extinction spectra of Au (blue solid line), CdSe/ZnS (black solid line), and plasmon-coupled CdSe/ZnS (black dash line), and the normalized fluorescence spectra of CdSe/ZnS in water (olive solid line) PMMA-CdSe/ZnS-PMMA-quartz plate (green solid line), and PMMA-CdSe/ZnS-PMMA-Au-quartz plate (red solid line). The fluorescence peak of colloidal SQDs in water was placed at ~546 nm with a stark shift of ~29 nm, which indicates the

intrinsic quantum efficiency ($\eta_{int} \sim \lambda_{Abs} / \lambda_{Fl}$) of ~95%. The fluorescence peaks from SQD layer with and without plasmon coupling were exhibited at ~539.8 and ~539.3 nm, respectively, without any major spectral changes. However, the fluorescence peaks from SQD layer on the PMMA with and without plasmon coupling displayed ~6.7 and ~6.2 nm blue shift, respectively, compared to the fluorescence peak of colloidal quantum dots. The colloidal SQDs in solutions exhibited a red shift of the exciton absorption peak with higher concentrations, and a blue shift with lower concentrations. The red shift was due to homo energy transfer from the higher energy of smaller SQDs to the lower energy of bigger SQDs for relatively high concentration. The blue shift was possibly because of the reduction of energy transfer between SQDs.[6] It implied that the SQDs on the PMMA were well distributed.

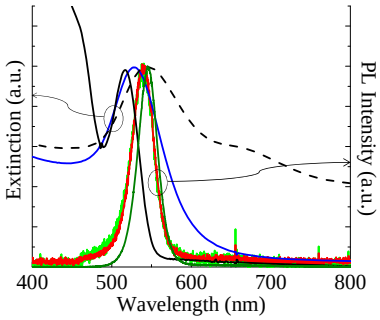

Figure 4. Extinction spectra of colloidal CdSe/ZnS SQDs (black solid line), Au NPs (blue solid line), and PMMA/SQDs/PMMA/Au NPs on the quartz plate (black dash line). Fluorescence spectra of CdSe/ZnS SQDs in water (olive solid line), and SQDs without (green solid line) and with (red solid line) plasmon coupling on the quartz plate.

The decay time traces of CdSe/ZnS and plasmon-coupled CdSe/ZnS were shown in the figure 5, and the average lifetimes CdSe/ZnS with and without plasmon coupling were shown in the table 1. The decay times of CdSe/ZnS between a PMMA film and a quartz substrate without plasmon coupling were analyzed into three components of τ_1 ~2 ns, τ_2 ~11 ns, and τ_3 ~39 ns. The fast decay time component (τ_1 ~2 ns) was unchanged between the lifetimes of CdSe/ZnS and plasmon-coupled CdSe/ZnS. The fast lifetime component (τ_1) was possibly because of the direct energy transfer from a nearest-neighbor CdSe/ZnS to CdSe/ZnS nanoparticles,[7] rather than the possible contribution of a weak decay component of plasmonic Au nanoparticle emission in the green spectral region. The second decay component (~11.2 - ~13.7 ns) of amplitude average lifetime for CdSe/ZnS with plasmon coupling exhibited a small variations compared to that (~10.99 ns) of CdSe/ZnS without plasmon coupling. The second component lifetime of plasmon-coupled SQDs was similar to the decay time of CdSe/ZnS in thin films or on the glass.[8] The lifetime quenching and the photoluminescence efficiency reduction have been observed when the SQDs were cast into the thin films,[9] due to the increase of nonradiative rate. The longest decay time (τ_3 ~39 ns) was the exciton lifetime characteristic of an isolated CdSe/ZnS on the glass plate[10] or well-dispersed colloidal SQDs in base solutions. The exciton lifetime originated from

radiative decay within CdSe/ZnS. The longest decay component of CdSe/ZnS was completely quenched when the SQDs were coupled with plasmonic Au nanoparticles. It is evidenced by the fact that the plasmon and exciton coupling rate in the presented hybrid nanostructure was faster than that of non-radiative decay rate, even though the lifetime for plasmon-exciton coupling rate was not clearly resolved within the experiment condition. As the table 1 listed, the longest lifetime (~38.8 ns) with 7% amplitude of SQDs without plasmon coupling was completely quenched when the SQDs were coupled with plasmonic Au nanoparticles. The amplitude a_2 for the second component lifetime of plasmon-coupled SQDs were increased ~15% - ~24% compared to that of SQDs without plasmon coupling. The increment was possibly because of the reduction of non-radiative decay in the hybrid nanomaterials of plasmon-coupled SQDs. Meanwhile, the total PL intensity of hybrid nanostructure was enhanced up to ~9-fold compared to that of CdSe/ZnS without plasmon coupling. It suggests that the PL enhancement is possibly originated from large local field enhancement and additional resonant energy transfer and re-excitation process. The PL intensity gradually decreased as the interparticle distance was increased, but exhibited strong PL enhancement up to the coupling distance ~82 nm which was the largest distance for the hybrid optical materials.

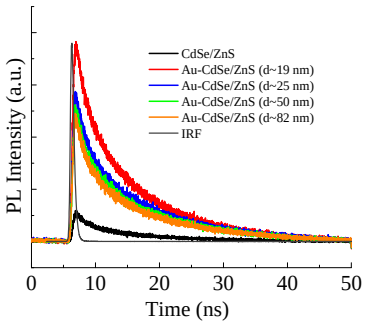

Figure 5. Decay time traces of CdSe/ZnS and plasmon-coupled CdSe/ZnS. The scanning area of fluorescence lifetime image was 80×80 μm^2.

Sample	***d(nm)***	a_1(%)	τ_1	a_2(%)	τ_2	a_3(%)	τ_3	χ^2	$\langle\tau\rangle_{amp}$	$\langle\tau\rangle_{Int}$	***I***
CdSe/ZnS		43	2.2	50	10.9	7	38.8	0.97	9.09	18.47	1.0
Au-CdSe/ZnS	~19	36	2.3	64	11.2			1.02	7.95	10.24	8.8
Au-CdSe/ZnS	~25	36	2.1	64	12.3			1.01	8.60	11.38	6.2
Au-CdSe/ZnS	~50	34	2.9	66	13.7			1.02	10.06	12.61	5.7
Au-CdSe/ZnS	~82	41	2.3	59	13			0.98	8.62	11.86	5.1

Table 1. Lifetime (unit in ns) analysis of CdSe/ZnS with and without plasmon coupling.

Apart from the time-resolved photoluminescence characteristics with the interparticle distance, the polarization-resolved PL spectroscopy also indicated an evidence of the coupling between the CdSe/ZnS emission dipoles and dipolar plasmon modes in the hybrid nanostructure. The polarization-resolved PL properties of hybrid plasmon-coupled CdSe/ZnS were characterized as shown in figure 6. The excitation source was a CW HeCd laser (Melles Griot, 45-MRM-803-120) operating at 325 nm at 40 mW. The PL of the hybrid nanostructure was collected using an optical fiber (Ocean Optics, P600-2-VIS-NIR), a long wavelength pass filter at 455 nm, and a spectrometer (Ocean Optics USB4000, Resolution: 1 nm). The laser excitation polarization was kept in same direction for all PL polarization measurements. The PL of CdSe/ZnS was uniformly distributed without plasmon coupling as shown in figure 6 (a). It was expected to observe that the normalized PL of plasmon-coupled CdSe/ZnS with the interparticle distance of ~25 nm was horizontally polarized as shown in figure 6 (b).[11] However, the PL of hybrid nanostructure with the interparticle distance of ~50 nm was de-polarized. It was possibly due to the weakening of dipolar interactions. Therefore, both time- and polarization-resolved PL studies of plasmon-coupled SQDs implied that the PL enhancement of hybrid nanostructure is originated from large local field enhancement, fast resonant energy transfer, and re-excitation process.

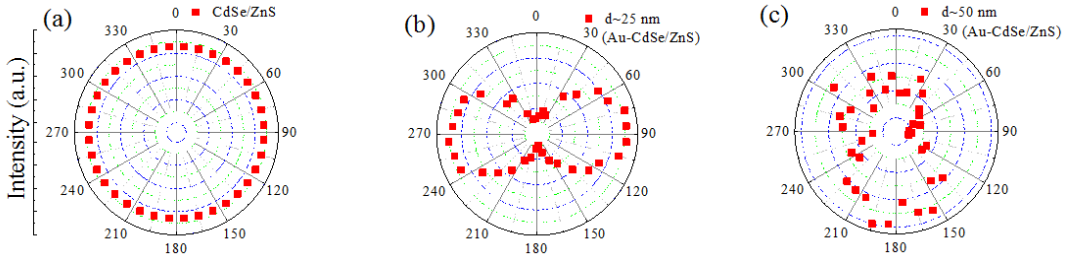

Figure 6. Polarization-resolved photoluminescence of CdSe/ZnS (a) without, and (b, c) with plasmon coupling.

Optical Spectroscopy of CdSe Quantum Dot-linked Lysozyme Protein Crystals

The optical spectroscopy of CdSe quantum dot (QD) and QD-linked lysozyme protein crystals include absorption, fluorescence, and lifetime measurements. Absorption spectra of QD and QD in protein crystals were measured with an UV-Vis spectrophotometer (Cary 50 Bio, Varian Inc.) in the spectral region from 250 to 800 nm with a scanning rate of 4800 nm/min. The optical path length of QD and QD in protein crystals with buffer salt base solution was 1 cm in a four-side clear cuvette. The fluorescence spectra of QDs and QD protein crystals were collected with a specrofluorometer (Cary Eclipse, Varian Inc.). The excitation source was a xenon flash lamp at ~470 nm with an excitation slit width of ~5 μm. The excitation irradiation was filtered out using a long wavelength pass (LWP) filter at ~495 nm. The slit width for fluorescence measurement was ~10 μm. The scanning range and rate of fluorescence spectra measurement were 500-700 nm and 600 nm/min. Fluorescence lifetime images (FLIM) were obtained on a confocal MicroTime 200 (Picoquant GmbH, Berlin) system coupled to an Olympus IX71 microscope

(Center Valley, PA). Fluorescence photons were gathered using a 60X water immersion objective (N.A 1.2, Olympus, Tokyo) from a sample dropped onto a 20x20 #1 coverslip (Menel Glauser, Braunschweig). As a light source, a pulsed laser (470 nm LDH-P-C470B) with a repetition rate of 10MHz was used. Fluorescence photons passed through a 30 μm confocal pinhole before being collected with a hybrid GaAsP photomultiplier detector (PMA Hybrid 40, Picoquant) and processed using the PicoHarp300 time-correlated single photon counting (TCSPC) module. The time-resolved fluorescence decay was collected through a 488-nm LWP filter before the pinhole to remove the scattered laser irradiation to the detector. The fluorescence-intensity average lifetimes of QDs and QD-linked protein crystals were estimated by a tail fitting of a multi-exponential decay function and a nonlinear least square function to the decay measurements using the SymPhoTime (v. 5.3.2) software package (Picoquant).

Figure 7 shows absorption and fluorescence spectra of QDs, QD-linked protein crystals, lysozyme, and buffer salt base solution. The lysozyme typically displays an absorption band around ~280 nm. The absorption spectrum of CdSe QDs displayed a strong blue shift of optical bandage compared to that (~718 nm) of CdSe bulk materials, and multiple peaks at ~483, 540, and 577 nm. The multiple absorption peaks indicate the discrete energy states of QDs with quantum confinement near the sizes at exciton Bohr radius (~5.8 nm). The absorbance of the first absorption peak at ~577 nm was ~0.195. The diameter and concentration of CdSe QDs were estimated to be ~3.8 nm and ~9.75×10^{-7} M with an extinction coefficient ~2×10^{5}/cm·M, respectively.[12] The fluorescence peak of CdSe QDs was placed at ~606 nm with a spectral Stark shift ($\Delta\lambda_S$) of ~29.5 nm. However, the distinct absorption peaks and a sharp bandedge with CdSe QDs were diluted or disappeared with QD-linked lysozyme protein crystals. In addition, the fluorescence intensity of QD-linked lysozyme protein crystals was strongly quenched compared to that of bare CdSe QDs. Therefore, the optical property changes of absorption and fluorescence spectra may imply the strong interaction between QDs with possible molecularization or crystallization of QD-assisted lattice separation in lysozyme protein crystals.

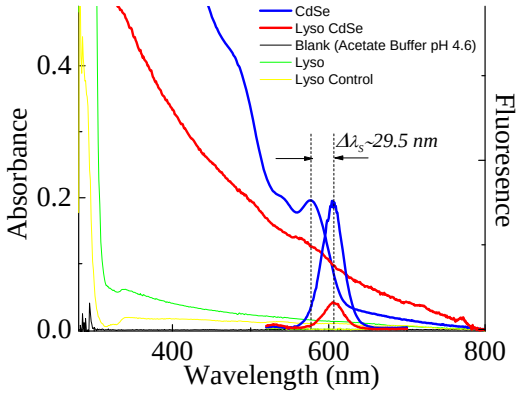

Figure 7. Optical spectra of CdSe QDs and QD-linked lysozyme protein crystals.

Figure 8 exhibits the lifetime images, fluorescence intensity decays, multi-exponential fittings, instrumentation response time, residual traces, and lifetime distributions for the CdSe QDs and the QD-linked lysozyme protein crystals. Figure 8 (a) and (b) clearly displayed the lifetime images of the colloidal CdSe QDs and the QD-linked lysozyme protein crystals. The lifetimes of CdSe QDs and QD-linked lysozyme protein crystals were analyzed with multi-exponential fitting. The least-square fit, χ^2, serves as serves as the optimization parameter, which is expected to be near 1.0 for a good lifetime fitting. The corresponding least-square fits of CdSe QDs and QD-linked lysozyme protein crystals were estimated to be ~1.029 and ~0.997 with the tail fittings, respectively. As the result, both samples exhibited triple exponential decays of the first, second, and third lifetime components. The fluorescence lifetimes of QDs were estimated to be ~1.413 ns with ~20.99% fractional intensities for the first decay components, ~6.003 ns with ~40.29% fractional intensities for the second decay components, and ~16.283 ns with ~38.72% fractional intensities for the third decay components. The fluorescence lifetimes of QD-linked lysozyme protein crystals were analyzed to be ~0.574 ns with ~53.09% fractional intensities for the first decay components, ~3.124 ns with ~33.58% fractional intensities for the second decay components, and ~14.088 ns with ~13.33% fractional intensities for the third decay components. The triple exponential decays of fast, medium, slow components may indicate the direct energy transfer from a nearest-neighbor CdSe to CdSe QDs, the energy transfer to surroundings, and the exciton lifetime characteristic of isolated or outer QDs on lysozyme protein, respectively.[13] The intensity averaged lifetimes of QDs and QD-linked lysozyme protein crystals were found to be ~13.04 ns and ~9.25 ns, respectively. As expected, the lifetime decay components and the intensity averaged lifetimes of QD-linked lysozyme protein crystals are shorter than those of QDs. Also, the probability (~53.09%) of fast decay component (~0.574 ns) of QD in protein crystals was higher than that (~1.414 ns with 20.99%) of QDs. These facts imply that the energy transfer between QDs in protein crystals was stronger than that between colloidal QDs. The strong energy transfer for QD in protein crystals could be occurred between the nearest QDs at each lattice position. Therefore, the shorter lifetimes of QD in protein crystals may support the possible QD coordination in protein-assisted crystals.

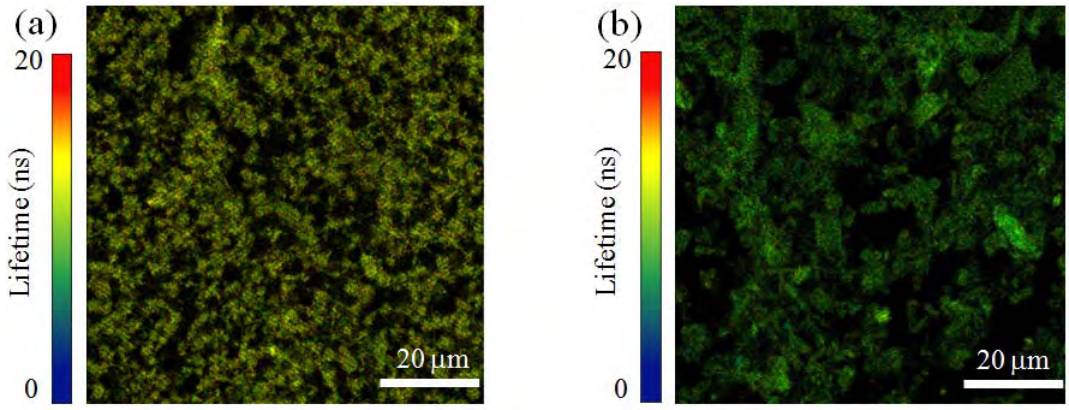

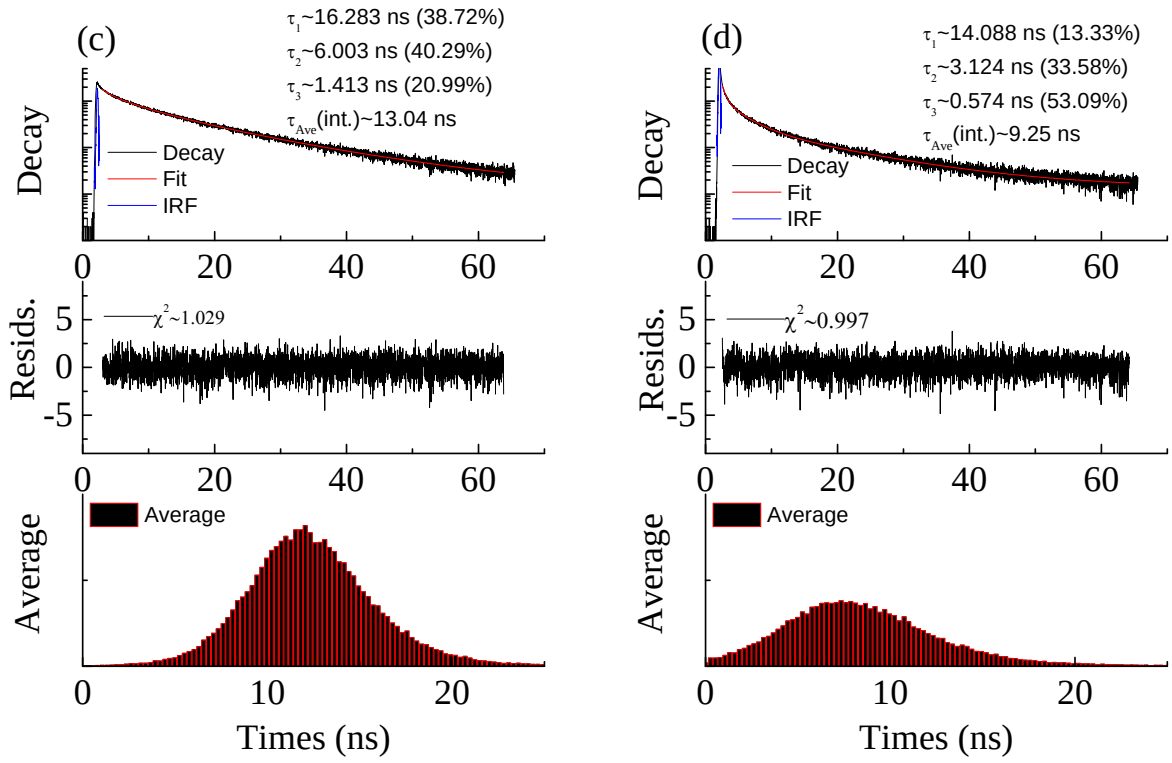

Figure 8. Lifetime images of (a) CdSe QDs and (b) QD-linked lysozyme protein crystals, and fluorescence intensity decays, residual traces, and lifetime distributions of (c) CdSe QDs and (d) QD-linked lysozyme protein crystals. Both QDs and QD-linked lysozyme protein crystals were placed on the cover slide for the lifetime measurements.

Time-resolved and temperature-dependent photoluminescence of ternary and quaternary nanocrystals of $CuInS_2$ with ZnS

Semiconductor nanocrystals (SNCs) are of great interest for various applications in optoelectronic devices, light emitting devices (LEDs),[14,15] and biological imaging[16,17] in visible and near-infrared spectral regions. The SNCs have a relatively good photostability compared to organic dyes which have a relatively strong photobleaching. The SNCs can be incorporated into electronic systems in opposition to solid insulators because of their semi-conductivity. It can be simply integrated with nano or micro photoelectronic and imaging devices because of their sizes in nanoscale. The semiconductors with sizes near the bulk Bohr radius display strong optical blue-shift and atom-like discrete energy states due to the quantum confinement of exciton electron-hole pairs within nanoscale boundary. The absorption bandedges and emission spectra of SNCs can be tuned by changing morphologies, compositions, and lattice strains or deformations. The large optical tunability of SNCs enables various photonic applications in a wide optical spectral region from visible to mid-infrared.

The optical SNCs may include binary, ternary, and quaternary II-VI, IV-VI, I-III-VI_2, and III-V compounds and coreshells with same or mixed compound groups. The II-VI SNCs of cadmium chalcogenide (Te, Se, and S)[18] and IV-VI SNCs of lead chalcogenide (Te, Se, and S)[19] with ZnSe (or ZnS) shell have high quantum yield and good color purity in the spectral region from visible to mid-infrared. However, the intrinsic toxicity of heavy metals, such as Cd, Pb, Te, or Se, in the SNCs limits their applications in bioimaging, LEDs, and photoelectronic devices. Considering chemical toxicity, I-III-VI_2 SNCs of copper indium disulfide, $CuInS_2$ (CIS), and III-V SNCs of InP[20,21,22] are relatively safer than cadmium or lead chalcogenide SNCs because they are less toxic.

Both SNCs of CIS and InP have wide optical tunability in the visible and near-infrared spectral region, and possess high quantum yield by surface capping with the higher bandgap SNC ZnS. The InP SNCs show relatively narrow spectral width in the visible spectral region, but wide spectral width over ~150 nm at full width at half maximum (FWHM) in the near-infrared spectral region. The wide size distribution could be one of the reasons for the wide emission spectral width. The CIS SNCs also have a wide spectral emission in the visible and near-infrared spectral regions. The large spectral width of CIS is mostly due to the wide size distribution as well as the multiple optical transitions in the CIS.

During the reporting period, time-resolved and temperature-dependent optical properties of bare CIS SNCs in ternary compound, CIS/ZnS coreshells, and ZnCIS quaternary compound were studied for prospective photonic applications. The time-resolved photoluminescence (PL) studies elucidate temporal dynamics of multiple optical transitions in CIS, CIS/ZnS, and ZnCIS SNCs. The temperature-dependent PL studies illustrate thermal quenching with activation ionization energies for the optical transitions in CIS, CIS/Zn, and ZnCIS SNCs. Therefore, the quantitative analysis of time-resolved and temperature-dependent PL properties along with absorption and photoexcitation characterization may provide a better approach to the realization of optoelectronic devices, light emitting devices (LEDs), and biological imaging applications.

All the chemicals were used as received from the chemical vendors. Oleylamine was received from Tokyo Chemical Industry (TCI) Co. Copper (I) iodide (CuI), indium (III) acetate ($InAc_3$), indium (III) iodide (InI_3) and 1-dodecanthiol (DDT) were purchased from Alfa Aesar. Zinc oxide (ZnO), sulfur powder (S), oleic acid (OA), octadecene (ODE), tributylphosphine (TBP) and diethyldithiocarbamide zinc (DECZn) were acquired from Aldrich.

All syntheses of SNCs were performed in non-coordinating solvent of ODE, and protected by N_2 gas.[18, 23] The schematic growth diagram of CIS, CIS/ZnS, and ZnCIS are depicted in figure 9. The synthesized SNCs were purified by following the literature procedures of hexane/methanol extraction, and precipitation in acetone.[18] The purified SNCs were re-dispersed in hexane, toluene, or chloroform for further characterization and experiments.

$CuInS_2$ (CIS) SNCs were prepared by heating a mixture of CuI, $InAc_3$ in DDT ([Cu] = [In] = 0.02 M) from room temperature to growth temperature between ~180 and ~250 °C at a rate of 10 °C/min.[24, 25, 26] The SNC growth was finished by removing the heating mantle to naturally cool the reaction. The size or luminescence spectrum of NCs was controlled by the growth temperature and reaction time.

$CuInS_2$/ZnS (CIS/ZnS) coreshells[26] were prepared by injecting a ZnO/OA/ODE solution to the CIS core particle solution. In this process, ZnO was converted to Zn oleate with OA in ODE. The Zn concentration was 0.1 M. The temperature for shell growth was ~210 ^oC to avoid the self-nucleation of ZnS.

$ZnCuInS_2$ (ZnCIS)[15,27,28] SNCs were prepared by heating the mixture, 2 ml of CuI/oleyamine solution ([Zn] = 0.045 M), 2 ml of InI3/oleylamine (InI_3/OAm) solution ([In] = 0.045 M), and 6 ml of DECZn/TBP/ODE ([DECZn] = 0.0167 M) in a flask, at a growth temperature between ~100 and ~230 °C.[26, 29] As alternative method, the ZnCIS can be prepared by heating the CIS/ZnS coreshells at ~210 ^oC for overtime between ~30 min. and ~1 hour.

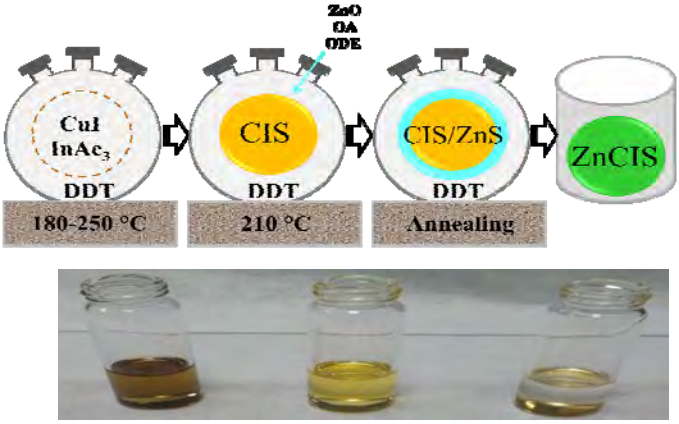

Figure 9. Schematic growth diagram of ternary CIS, CIS/ZnS core/shell, and quaternary ZnCIS.

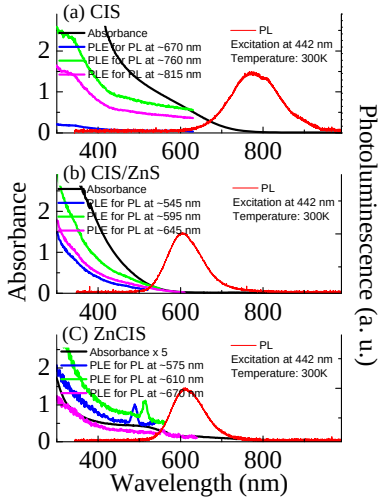

Figure 10. Absorption, PLE, and PL spectra of (a) CIS, (b) CIS/ZnS, and (c) ZnCIS. The absorption spectra tails stretched up to ~765 nm for CIS, ~590 nm for CIS/ZnS, and ~760 nm for ZnCIS. The PL peaks were shown at ~775 nm with ~140 nm in FWHM for CIS, ~605 nm with ~100 nm in FWHM, and ~611 nm with 90 nm in FWHM. The PLE peaks of ZnCIS were displayed at ~489, ~513, ~565 nm for monitoring the PL at ~575, ~610, ~670 nm, respectively.

Figure 10 shows absorption, PLE, and PL spectra of ternary compound CIS, CIS/ZnS coreshell, and quaternary compound ZnCIS. The absorption spectra have long trails without apparent peaks. However, they have a clear blue-shift from that of bulk CIS at ~810 nm which is related to quantum confinement with nanocrystal sizes near the bulk Bohr radius. The absorption tails stretched up to ~765 nm for CIS, ~590 nm for CIS/ZnS, and ~760 nm for ZnCIS. The PL peaks of SNCs displayed at ~775 nm for CIS, ~605 nm for CIS/ZnS, and ~611 nm for ZnCIS. The capping ZnS on CIS displayed strong blue shift of absorption and PL spectra. The spectral blue shifts of CIS have been described with the bandgap widening of smaller particle sizes or copper deficiency,[30, 31] and compressive strain by lattice mismatch between core and shells.[32, 33, 34, 35, 36] In the case of CIS/ZnS, Kim,[32] Smith,[33] and their co-authors explained that the spectral blue shift is due to the compressive stress by lattice mismatch between core and shell layers, because of a smaller lattice parameter of ZnS than that of CIS. Uehara et. al.[30] illustrated the blue shift with partial alloying of ZnS into CIS core materials. Li et al.[37] described the blue shift with potential etching of core materials and increased spatial confinement. Park and Kim[38] elucidated the blue shift with size reduction through cation exchange. The capping of ZnS on CIS has been used to enhance PL efficiency by removing non-radiative recombination centers, however, the lattice mismatching between core and shell might degrade the optical properties.[39] The alloying ZnS into CIS displayed a slight spectral redshift of PL, and exhibited again the absorption tails at the longer wavelength. Kim et al.[32] illustrated the spectral redshift with the tensile stress in the SNCs. The PL spectral width changes from ~140 nm, ~100 nm, to ~90 nm in FWHM for CIS, CIS/ZnS, and ZnCIS can be possibly attributable to the reduction of surface-trapped state, the compressive stress by lattice mismatching, and the potential etching of core materials through cation exchange. The ZnCIS displayed distinct PLE peaks at ~489, ~513, ~565 nm when PL was monitored at ~575, ~610, ~670 nm, respectively, in contrast of the broad PLE spectra of CIS and CIS/ZnS for monitoring three represented PL wavelengths. The distinct PLE peaks from ZnCIS imply that the existence of spatial confinement increase by core material etching and size reduction through cation exchange.[37, 38, 40] The PL origin of CIS SNCs was illustrated with surface-trapped state recombination and defect-related donor-acceptor (D-A) recombination.[25, 41] Zhong et al.[25] described that the surface-trapped states for electrons and holes are related to the chalcogen atoms and absorbents on the SNC surface. Komarala,[42] Castro,[41] Ueng[43] and their co-authors illustrated the defect-related D-A recombination of the potential transitions, which the shallow donor state relates to sulfur vacancy (V_s), and a deep donor state relates to either indium interstitial (In_i) or indium atom in the copper vacancy (In_{Cu}) below the conduction band (E_c); and the acceptor state is related to indium-rich (In_{Cu}) as a deep state and copper-rich (Cu_{In}) as a shallow state above the valence band (E_v). Ueng and Hwang[43] explained that the interactions among the multi-energy levels with such intrinsic defects would significantly influence each other. Therefore, the time-resolved PL studies in different spectral regions for CIS, CIS/ZnS, and ZnCIS provide the temporal emission properties of surface-related recombination and defect-related D-A recombination of exciton pairs. The temperature-dependent PL studies reveal the emission quenching properties and the interactions between multilevel energy states including surface-trapped states and defect-related donor and acceptor states. The time-resolved and temperature-dependent studies of the PL in figure 10 are shown in figures 11 and 12, respectively, which provide a better understanding the optical dynamics of CIS, CIS/ZnS, and ZnCIS for efficient photonic devices and bioimaging applications.

In this report, the temporal PL decays of CIS, CIS/ZnS, and ZnCIS were characterized at three different PL spectral regions of shorter, center, and longer wavelengths at ~660, ~760, and ~815 nm for CIS, ~545, ~595, ~645 nm for CIS/ZnS, and ~570, ~610, and ~670 nm for ZnCIS SNCs to analyze the contributions of surface-related recombination, shallow and deep defect-related D-A transition to the selected spectral regions, which were assigned by Komarala,[42] Castro,[41] Ueng[43] and their co-authors. In contrast to the direct recombination of electrons and holes in the quantized conduction and valence bands and the transitions from surface-trapped states in II-VI SNCs, the surface-related recombination and defect-related D-A transitions are dominant in CIS SNCs.[16, 44] In II-VI SNCs of cadmium chalcogenide, the energy of bandgap transition is higher than that of surface-trapped state transition. In CIS SNCs, the energy of surface-related transitions is higher than that of defect-related D-A transitions. The emission lifetimes of surface-related and defect-related D-A transitions in CIS, CIS/ZnS, and ZnCIS were de-convoluted into three exponential decay components with the best fits with near unity residual traces. Zhong,[25] Komarala,[42] and their co-authors explained that the fast decay component (τ_1) is assigned to the emission transition from surface-trapped states, and the slow decay components (τ_2 and τ_3) are attributed to the defect-related D-A transitions. Nose et. al[45] reported the existence of the interface-trapped state between core and shell which is similar to the surface-trapped state with core materials. Therefore, in the case of CIS/ZnS, the fast decay component (τ_1) can be attributed to the interface-trapped state. Enzenhofer,[46] Castro, [41] and their co-authors described that the emission decay from surface-trapped state is relatively fast because it is usually shallow compared to the defect-related donor states. Therefore, the time-resolved PL measurement explains the three types of PL radiative transitions in the prepared ternary and quaternary compound SNCs.

Figure 11 shows PL intensity decays, residual traces, and exponential decay components of fractional emission intensities of (a) CIS at ~660 nm, (b) CIS at ~760 nm, and (c) CIS at ~815 nm in toluene. The longest lifetime (τ_3) of CIS in toluene is distributed over the entire spectrum with the largest decay amplitude fractions of ~69.13% at ~660 nm, ~79.66% at ~760 nm, and ~84.89% at ~815 nm among the three decay transitions. The τ_3 lifetimes was ~366.50 ns at ~815 nm, ~304.20 ns at ~760 nm, and ~215.14 ns at ~660 nm. The longer lifetime and larger decay amplitude fraction at longer wavelength indicate that the deep defect-related D-A transition is related to the longer wavelength (or lower energy) region as it is expected. It also implies that the wave function related to deep defect-related D-A transition is widely spread over the entire PL spectral region, but the lifetime is shortened and the decay amplitude fraction is reduced at the shorter wavelength regions. Hamanka et al.[44] described that the binding energies between donor and acceptor in SNCs is modified by the Coulomb interaction, and the transition probability between nearby pairs is higher than that between distant pairs. It implies that the nearby pairs have a shorter lifetime than that of the distant pairs. The medium lifetime (τ_2) of CIS is spread over with the decay amplitude fractions of ~28.13% at ~660 nm, ~19.67% at ~760 nm, and ~14.88% at ~815 nm. The τ_2 decay has larger amplitude fraction and shorter lifetime at shorter spectral region, but smaller amplitude fraction and longer lifetime at longer spectral region. It implies that the shallow defect-related donor level is closely located to the surface-trapped states in the CIS SNCs. The shortest lifetime (τ_1) of CIS is located all over the entire spectral region with the decay amplitude fractions of ~2.74% at ~660 nm, ~0.67% at ~760 nm, and ~0.23% at ~815 nm. The shortest lifetime can be explained by the strong PL quenching with relatively small activation ionization energy at lower temperatures, which can be explained with

temperature-dependent PL studies, and activation ionization energy. The τ_1 decay has larger amplitude fraction and longer lifetime at shorter spectral region, but smaller amplitude fraction and shorter lifetime at longer spectral region as it is expected. At the same time, the broad spectral contribution of each radiative transition (τ_1, τ_2, and τ_3) also explains the large emission spectral width of CIS SNCs.

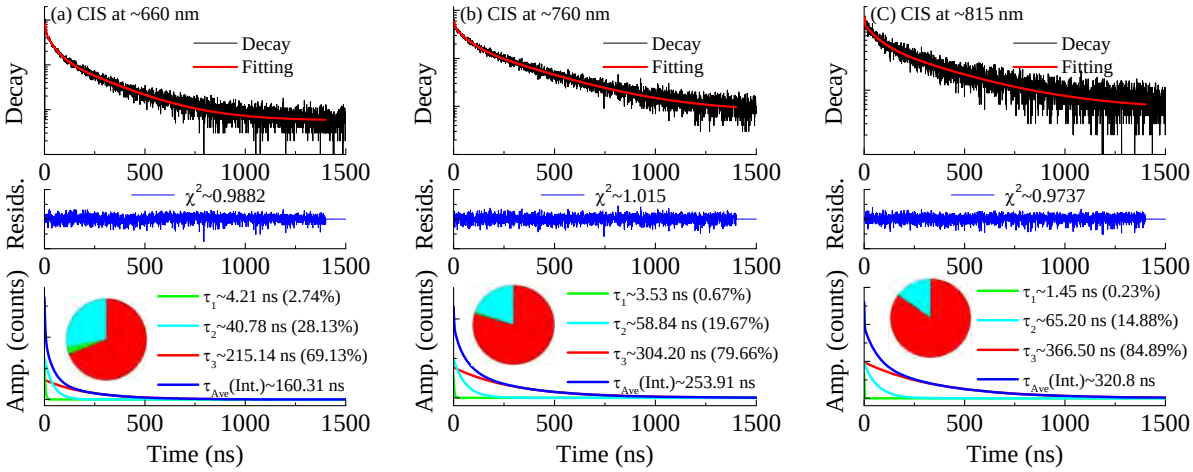

Figure 11. Emission intensity decays, residual traces, and exponential decay components of fractional emission intensities of (a) CIS at ~660nm, (b) CIS at ~760nm, and (c) CIS at ~815nm in toluene.

Figure 12 shows emission intensity decays, residual traces, and exponential decay components of fractional emission intensities of (a) CIS/ZnS at ~545 nm, (b) CIS/ZnS at ~595 nm, and (c) CIS/ZnS at ~645 nm in toluene. The three decay transitions of CIS/ZnS in toluene display similar behaviors of decay amplitude fractions and lifetime distributions at different spectral regions as those with CIS in toluene, except the longer lifetime of τ_1 at longer spectral region than that at shorter spectral region. Also, the averaged lifetime of CIS/ZnS is reduced compared to that of CIS, mainly due to the shortening of τ_3 lifetime with CIS/ZnS. Both lifetime changes with CIS/ZnS may be due to the implicit interplay of compressive strain by lattice mismatch between core and shells, and the initiation of partial cation exchange Zn^{2+} with either Cu^{+} or In^{3+}. Figure 12 also shows the temporal decay characterization of PL emissions (d) CIS/ZnS_{545nm}, (e) CIS/ZnS_{595nm}, and (f) CIS/ZnS_{645nm} on a micro cover glass. As expected, the τ_1 of CIS/ZnS on the micro-glass displays longer lifetime and higher amplitude fractions, because of the arising contribution of surface-trapped states.

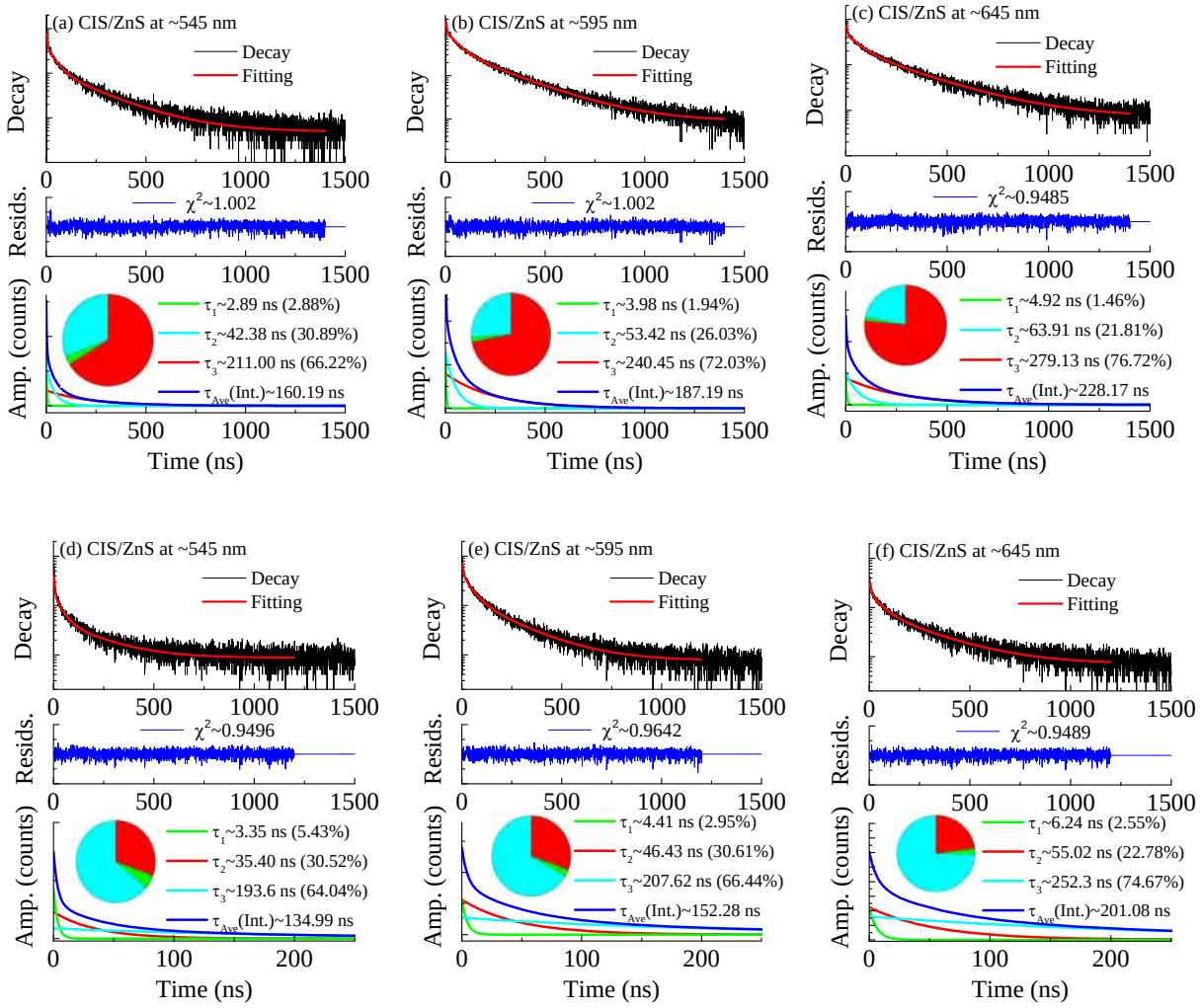

Figure 12. Emission intensity decays, residual traces, and exponential decay components of fractional emission intensities of (a) CIS/ZnS at ~545nm, (b) CIS/ZnS at ~595nm, and (c) CIS/ZnS at ~645nm in toluene, and (d) CIS/ZnS at ~545nm, (e) CIS/ZnS at ~595nm, and (f) CIS/ZnS at ~645nm on a cover glass.

Figure 13 shows emission intensity decays, residual traces, and exponential decay components of fractional emission intensities of (a) ZnCIS at ~570 nm, (b) ZnCIS at ~610 nm, and (c) ZnCIS at ~670 nm in toluene. The significant shortenings of τ_2 and τ_3 lifetimes indicate that the modification of defect-related D-A transition is due to partial cation exchanges. The large fractional emission intensities of τ_1 at ~570 nm and ~610 nm imply the development of surface-trapped state after ZnS shells smear into the core at the higher and longer synthesis temperature and time.

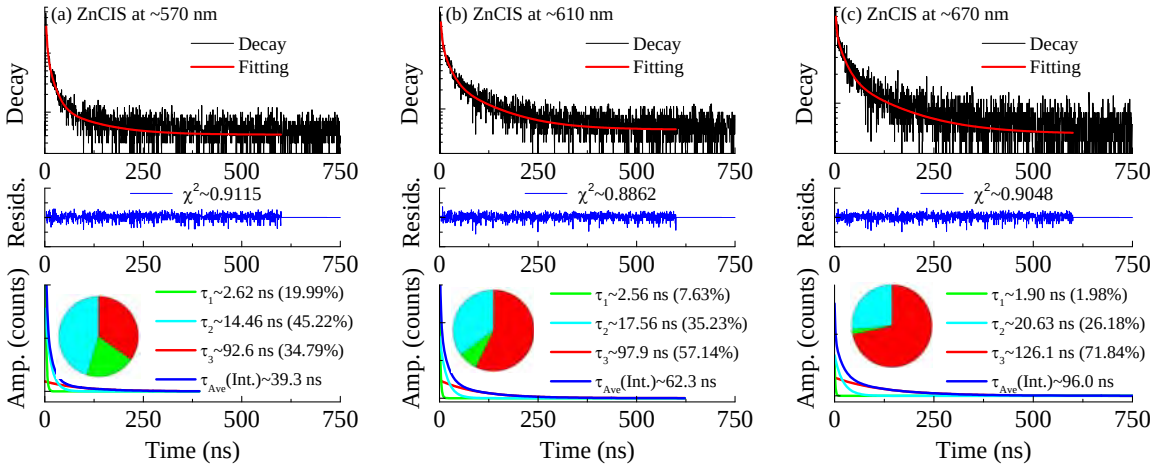

Figure 13. Emission intensity decays, residual traces, and exponential decay components of fractional emission intensities of (a) ZnCIS at ~570nm, (b) ZnCIS at ~610nm, and (c) ZnCIS at ~670nm in toluene.

Figure 14 shows the temperature-dependent PLs of CIS, CIS/ZnS, and ZnCIS at the sample temperatures from 6K to 300K. The temperature-dependent spectral widths (FWHM) of PLs were changed from ~135 nm to ~141 nm for CIS, from ~101 nm to ~98 nm for CIS/ZnS, and from ~90 nm to ~93 nm for ZnCIS by changing the sample temperatures from 6K to 300K. The spectral narrowing is probably due to the reduction of surface-trapped states, the compressive stress by lattice mismatching, and the potential etching of core materials through cation exchange. The temperature-dependent PL peak changes or variations were from ~781 nm to ~768 nm for CIS, from ~594 nm to ~602 nm for CIS/ZnS, and from ~609 nm to ~610 nm for ZnCIS. The spectral blue shift with CIS/ZnS and ZnCIS compared to that of CIS is attributed to the compressive stress by lattice mismatching between core and shell layers, and the increased spatial confinement with the etching of core materials and size reduction through cation exchange.[33, 37, 38, 40] The spectral variations with temperature changes also can be related to the thermal activation energies as plotted in figure 15.

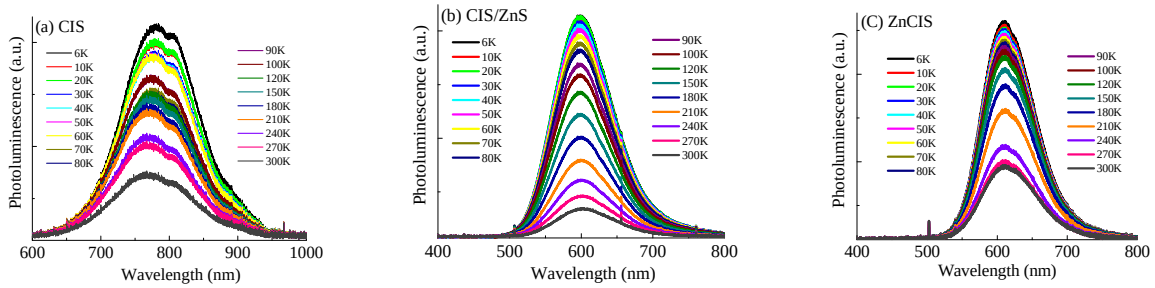

Figure 14. Photoluminescence of (a) CIS, (b) CIS/ZnS, and (c) ZnCIS.

Figure 15 shows the thermal quenching properties of PLs from CIS, CIS/ZnS, and ZnCIS, which are plotted as the integrated intensities as a function of inverse temperature of samples. The activation ionization energies of surface-related and defect-related states can be determined from the thermal quenching of PL measurement,

$$I_{PL} \sim \frac{1}{1 + T^{3/2} \sum_i C_i \exp\left(-E_{act,i} / k_B T\right)}, \quad (1)$$

where I_{PL} is the integrated PL intensity, T is the sample temperature, C_i is the fractional amplitude of activation ionization energy ($E_{act,i}$), and k_B is the Boltzman's constant.[47] The fitting parameters were $E_1 \sim 0.05\,meV$ with $C_1 \sim 2\times10^{-4}$ and $E_2 \sim 0.5\,meV$ with $C_2 \sim 3\times10^{-4}$ for CIS SNCs; $E_1 \sim 3\,meV$ with $C_1 \sim 5\times10^{-4}$ and $E_2 \sim 15\,meV$ with $C_2 \sim 5\times10^{-4}$ for CIS/ZnS SNCs; and $E_1 \sim 1.5\,meV$ with $C_1 \sim 3\times10^{-4}$ and $E_2 \sim 15\,meV$ with $C_2 \sim 2\times10^{-4}$ for ZnCIS SNCs. The fitting sensitivity on PL quenching behavior by the deep-defect level E_3 or deeper defect-related states could not be caught with the given numerical fitting within the temperature range from 6K to 300K. For the CIS SNCs, E_1 and E_2 are relatively shallow states, and may be assigned to the surface-trapped states which can be related to the chalcogen atoms and adsorbents on the CIS SNC surface.[25] For the CIS/ZnS SNCs, E_1 and E_2 can be assigned to the interface-defect related state,[45] similar to the surface-trapped state with the core materials, and shallow defect-related donor state, respectively. For ZnCIS SNCs, E_1 and E_2 can be assigned to the surface-trapped state, and the shallow defect-related donor state, respectively. The experimental results, shown in figure 15, for the thermal activation-ionization energies of surface-trapped states and defect-related donor states with CIS, CIS/ZnS, and ZnCIS SNCs agree with Komarala[42] and co-authors' description. According to Komarala's description, the surface-trapped electrons are thermally active, and can easily escape from the emission sites even at low temperatures, but the trapped electrons at intrinsic defect-related states may not be easily able to get away at low temperatures due to the strong Coulomb interaction between the charge carriers. Therefore, the shorter lifetime of surface-trapped state at room temperatures than that of defect-related D-A can also be explained by the thermally active surface-trapped electrons and the strong Coulomb attraction between defect-related charge carriers.

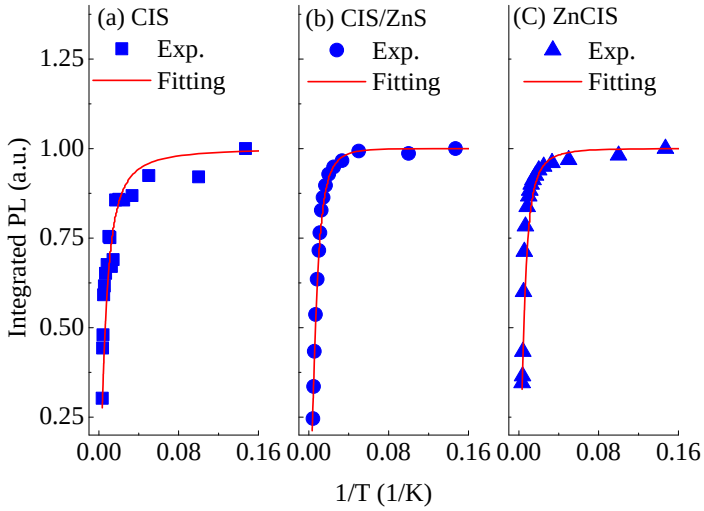

Figure 15. Thermal quenching properties of PLs from (a) CIS, (b) CIS/ZnS, and (c) ZnCIS.

In conclusion, the time-resolved PL studies of ternary and quaternary compound CIS, CIS/ZnS, and ZnCIS SNCs indicate the existence of a surface-trapped state, interface defect-related state, and intrinsic defect-related state. The shorter lifetimes are assigned to the surface-trapped state or interface defect-related state, and the longer lifetimes are related to the intrinsic defect-related donor-acceptor transitions. The shorter lifetime at the surface-trapped state or interface defect-related state at room temperature can be explained by the strong PL quenching with relatively small activation ionization energy even at lower temperatures. The electrons at intrinsic defect-related states have relatively longer lifetimes because they are thermally stable due to strong Coulomb interaction between the charge carriers. Both shorter and longer lifetimes are widely distributed at the entire PL spectra. It implies that all transitions from surface-trapped states, interface defect-related states, and intrinsic defect-related states contributed to the PL from CIS, CIS/ZnS, and ZnCIS SNCs. The spectral blue shift and spectral narrowing with CIS/ZnS and ZnCIS compared to that of CIS are assigned to the compressive stress by lattice mismatching between core and shell layers, and the increased spatial confinement with the etching of core materials and size reduction through cation exchange. The shortening of longer lifetimes of intrinsic defect-related states for CIS/ZnS and ZnCIS is attributed to the modification of defect-related transition through cation exchange.

Optical Properties of $CuInS_2$/ZnS Coreshells for Hybrid White LEDs

Light emitting devices (LEDs) are a key element in the photonic and optoelectronic devices including optical displays, room lighting, cell phones, motor vehicle head lights and indicators, traffic lights, and many more. The spectral purity or distribution is an important optical property of materials for developing photonic and optoelectronic devices. The broad spectral distribution is more important than the spectral purity for white light application of room lighting and motor vehicle head lights by replacing the filament bulbs for energy saving and lifetime, while the spectral purity is more important than the spectral distribution for the photonic applications of

traffic light, cell phone, and optical displays. The broad spectral distribution, wide optical tunability, and good photostability are essential optical properties for developing white LEDs in addition to the materials non-toxicity and robustness. Semiconductor nanocrystals (SNCs) are of significant interest in developing LEDs[48,49,50] because of their wide optical tunability and good photostability. The quantum confinement in the SNCs with sizes near the bulk Bohr radius (~4 nm) provides the wide optical tunability with strong blue-shift of optical bandgap.[51] The SNCs have good photostability with less photobleaching compared to the organic materials. The II-VI SNCs have a wide optical tunability, good photostability, and high color purity, but heavy metals and narrow spectral width is undesirable parameters for white LED development.[52] The I-III-VI_2 SNCs have a broad emission spectral width, wide optical tunability, and good photostability in addition to no-toxicity related to the heavy metals. Therefore, the I-III-VI_2 SNCs are excellent optical materials for hybrid white LED development.

The emission of II-VI SNCs mainly comes from the exciton pair recombination in the conduction and valence bands, and possibly the transitions from/to surface-trapped states just below the conduction band or above the valence band.[53] The optical tunability and blue-shift of SNCs with sizes near the exciton Bohr radius are explained by the Coulomb interaction between the exciton pair for II-VI SNCs or/and between donor-acceptor (DA) pair for I-III-VI_2 SNCs. The emission of I-III-VI_2 SNCs comes from the optical transitions related surface-trapped states for core materials, interface-trapped state for coreshells, shallow- and deep-trapped DA states.[54] The interface-trapped state, shallow- and deep-trapped DA states are correlated to the emissions at the higher, intermediate, and lower energy spectral region respectively.[55] However, the numerous interface, interstitial and vacancy on/in the large numbers of coreshells lead to the broad optical spectrum, and even overlap all emissions from the interface-trapped state and defect-related DA-trapped state.[56,57,58]

In this article, two selective I-III-VI_2 coreshells of CIS/ZnS_{665nm} and CIS/ZnS_{555nm} with photoluminescence (PL) peaks ~555 nm or ~665 nm are utilized for the hybrid white LED development. The temperature-dependent and time-resolved PL studies on the CIS/ZnS_{665nm} coreshells reveal the contributions of interface-trapped state and defect-related DA-trapped state to the PL spectra, while the optical studies on the CIS/ZnS_{555nm} coreshells illustrate the modification of PL decays and spectral symmetry. Finally, the time-resolved and temperature-dependent PL studies of CIS/ZnS_{665nm} and CIS/ZnS_{555nm} describe the optical origins of better spectral covering and spectral coupling for developing hybrid white LEDs, where the SNCs are stacked on the blue LEDs for the excitation as well as the spectral coupling in the entire visible spectral region.

Figure 16 shows absorption, PL and PLE spectra of CIS/ZnS coreshells. The absorption spectra of coreshells have a strong blue-shift from the optical bandgap (~1.5 eV/~827 nm) of bulk CIS due to quantum confinement.[59] The PLE spectra of CIS/ZnS_{555nm} displayed broad shoulders at ~470 nm and ~480 nm for the monitoring PL wavelengths at ~525 nm, ~550 nm, and ~600 nm. It indicates the broad spectral contribution of interface-trapped state and defect-related DA trapped states to the PL of CIS/ZnS. However, the broad PLE shoulder disappeared or was reduced for CIS/ZnS_{665nm} which implies that the wide size distribution and various types of defect play the role in the further spectral broadening of PLE.[60] The absorption and PLE spectra of CIS/ZnS did not exhibit the multiple distinct peaks which could be observed from the II-VI

SNCs with sizes near bulk Bohr radius as the result of quantum confinement.[61] The optical transitions in II-VI SNCs are mainly related to the exciton pair recombination in the conduction and valence bands, and surface-trapped states, while those of I-III-VI_2 are related to the surface/interface-trapped state and defect-related DAP recombination.[62,63] The PL spectra of CIS/ZnS_{555nm} and CIS/ZnS_{665nm} exhibited the peaks at ~555 nm and ~665 nm, which are attributed to the interface-trapped states, shallow- and deep trapped donor-acceptor (DA) states. The PL spectral widths of CIS/ZnS_{665nm} and CIS/ZnS_{555nm} at the materials temperature of 300K are ~115 nm at FWHM (~615 nm - ~730 nm) and ~100 nm at FWHM (~520 nm - ~620 nm) respectively. The PL width (~115 nm at FWHM) of CIS/ZnS_{665nm} has the wider spectral covering compared to that (~100 nm at FWHM) of CIS/ZnS_{555nm}. The PL from CIS/ZnS_{555nm} has the better spectral coupling with the blue excitation for generating white light in the visible spectral region while CIS/ZnS_{665nm} has the undesired infrared emission which is similar to the previous reports.[64] The asymmetry of PL spectrum and the reduced spectral width of the CIS/ZnS_{555nm} compared to the PL properties of CIS/ZnS_{665nm} are due to the higher contributions of interface-trapped states and shallow-trapped DA states in the lower wavelength spectral region and the less size-dependent on confinement of the deep-trapped state. Therefore, the time-resolved and temperature-dependent PL studies of CIS/ZnS_{665nm} and CIS/ZnS_{555nm} is required to explain the optical origins of spectral covering and coupling for developing hybrid white LEDs.

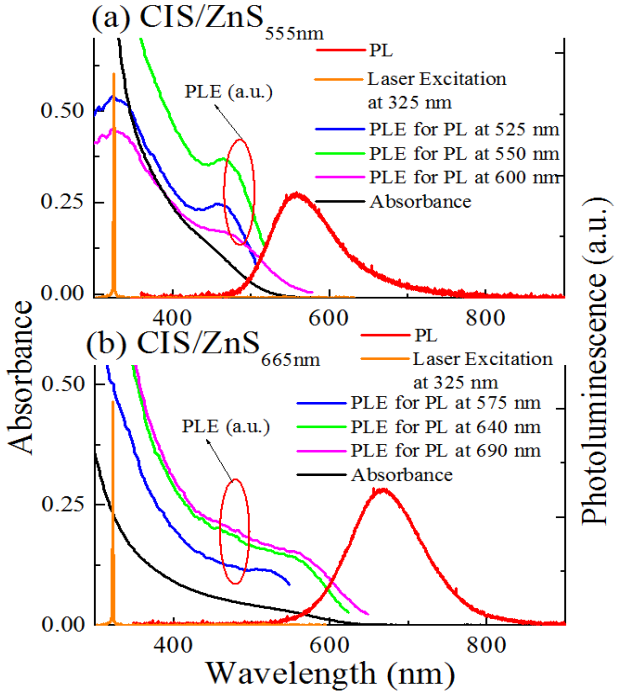

FIG 16. Absorption, PLE, and PL spectra of (a) CIS/ZnS_{555nm} and (b) CIS/ZnS_{665nm}.

Figure 17 shows the PL decays (top), residual traces (middle), and decay components (bottom) from CIS/ZnS_{665nm} at shorter wavelength 575 nm (a), center wavelength 640 nm (b), and longer wavelength 690 nm (c). The PL at 575 nm have three exponential decay times with fast (τ_1), intermediate (τ_2), and slow (τ_3) components of ~4.8 ns, ~17.8 ns, and ~85.7 ns with the fractional amplitudes of 62.3%, 34.3%, 3.4%, respectively. The PL decays at 640 nm have fast (τ_1), intermediate (τ_2), and slow (τ_3) components of ~6.7 ns, ~35.8 ns, and ~131.8 ns with the fractional amplitudes of 48.0%, 41.6%, and 10.3%, respectively. The PL decays at 690 nm have

fast (τ_1), intermediate (τ_2), and slow (τ_3) components of ~15.6 ns, ~65.4 ns, and ~188.0 ns with the fractional amplitudes of 34.1%, 43.5%, and 22.5%, respectively. The averaged lifetimes of three exponential decays of CIS/ZnS_{665nm} are ~12.0 ns, ~31.7 ns, and ~76.0 ns at the PL wavelengths 575 nm, 640 nm, and 690 nm, respectively. The larger fractional amplitude of the fast life time (τ_1)at the shorter wavelength indicates that the fast decay component of PL is related to the interface-defect state. The large fractional amplitude increase at longer wavelength for the slow decay (τ_3) component suggests that the slow decay is related to defect-related deep-trapped DA state. Then, the intermediate (τ_2) decay component in the broad spectral region is possibly assigned to the shallow-trapped DA state which is strongly overlapped with interface-tapped state and deep-trapped state. The fractional amplitude of fast (τ_1) decay component is decreased at longer wavelength, and that of intermediate (τ_2) and slow (τ_3) components is increased at longer wavelength. The fast (τ_1) and intermediate (τ_2)decay components have large fractional amplitudes in the entire spectral region. It implies that interface-trapped state and shallow-trapped DA state provide the major contribution to the PL.

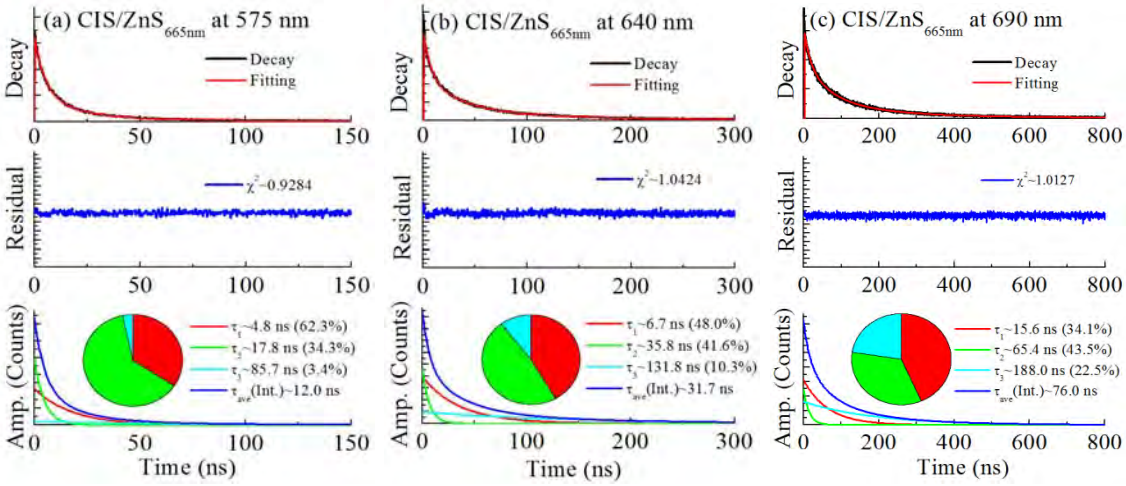

FIG. 17. Emission intensity decays, residual traces, and exponential decay components of fractional emission amplitudes of CIS/ZnS_{665nm} at (a) ~575nm, (b) ~640 nm, and (c) ~690 nm on the micro-cover glass.

Figure 18 shows the PL decays (top), residual traces (middle), and decay components (bottom) from CIS/ZnS_{555nm} at shorter wavelength 525 nm (a), center wavelength 550 nm (b), and longer wavelength 600 nm (c) to analyze the contributions of interface defect-relate states, shallow- and deep-trapped defect-related DA states. The PL at 525 nm have three exponential decay times with fast (τ_1), intermediate (τ_2), and slow (τ_3) components of ~17.3 ns, ~116.3 ns, and ~428.9 ns with the fractional amplitudes of 48.8%, 40.3%, 10.9%, respectively. The PL decays at 550 nm have fast (τ_1), intermediate (τ_2), and slow (τ_3) components of ~23.5 ns, ~160.8 ns, and ~565.8 ns with the fractional amplitudes of 49.8%, 43.4%, and 7.9%, respectively. The PL decays at 600 nm have fast (τ_1), intermediate (τ_2), and slow (τ_3) components of ~20.2 ns, ~ 184.0 ns, and ~575.4 ns with the fractional amplitudes of 42.2%, 45.6%, and 12.2%, respectively. The fractional amplitudes of fast (τ_1) PL decay are slightly decreased, but those of intermediate

(τ_2) PL decay are slightly increased. However, both fractional amplitudes of fast (τ_1) and intermediate (τ_2) decays have the major contributions to the PL, and widely distributed in the entire spectral region. It indicates that the interface-trapped state and shallow-trapped DA state are strongly overlapped. The average lifetimes of three exponential decays of CIS/ZnS_{555nm} are ~101.9 ns, ~124.3 ns, and ~162.3 ns at the PL wavelengths 525 nm, 550 nm, and 600 nm, respectively. The averaged PL lifetimes of CIS/ZnS_{555nm} are longer than those of CIS/ZnS_{665nm}. It implies that CIS/ZnS_{555nm} has less PL quenching through non-radiative decay process.

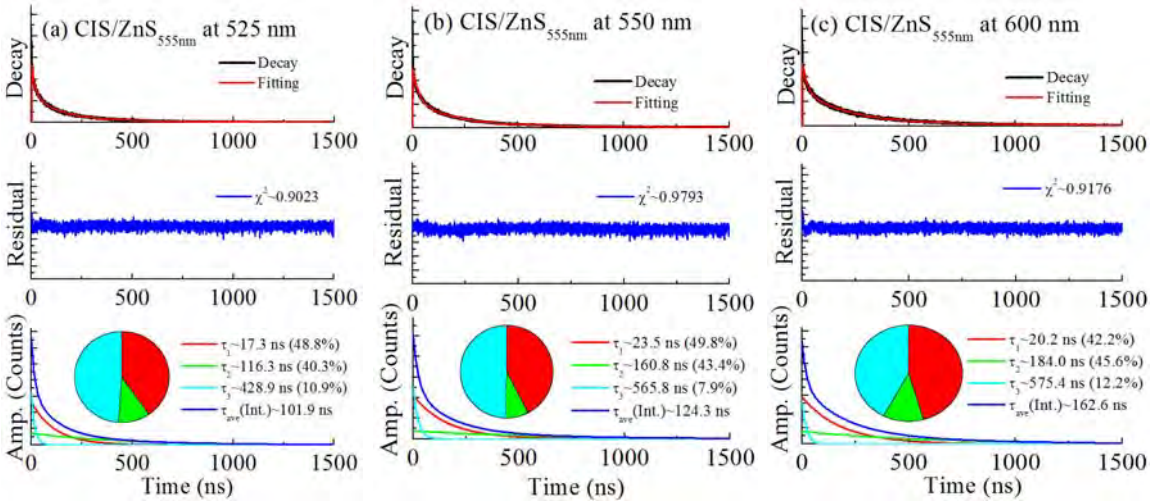

FIG. 18. Emission intensity decays, residual traces, and exponential decay components of fractional emission amplitudes of CIS/ZnS_{555nm} at (a) ~525nm, (b) ~550 nm, and (c) ~600 nm on the micro-cover glass.

The thermal quenching properties of PL from CIS/ZnS_{555nm} and CIS/ZnS_{665nm} make further confirmation on the implication of defect-related interface-trapped state, shallow- and deep-trapped DA states to PL distribution. The temperature dependent PLs from CIS/ZnS_{555nm} (a) and CIS/ZnS_{665nm} (b) are shown in figure 19. The PL of CIS/ZnS_{555nm} has asymmetric spectral distribution, while the PL of CIS/ZnS_{665nm} has symmetric spectral distribution. It implies that the deep-trapped DA states are less size-dependent on the confinement compared to the shallow-trapped DA state and defect-related interface state. It is well known that the surface/interface defects of nanomaterials are increased as the relative surface area per volume is increased by decreasing the size.[65] The temperature-resolved spectroscopy shows that the PL from the interface-trapped state and shallow-trapped DA state has less thermal quenching and the PL at longer wavelength from the deep-trapped DA states has stronger thermal quenching. The PL peak of CIS/ZnS_{665nm} is shifted from ~670 nm to ~665 nm as the temperature is increased from 6K to 300K. The PL irradiance reduction of CIS/ZnS_{555nm} at longer wavelength region is faster than that at shorter wavelength region as the temperature is increased. It implies the existence of the stronger thermal ionization and phonon-assisted non-radiative decay at the deep-trapped DA states with the relatively stronger Coulomb interaction.[66]

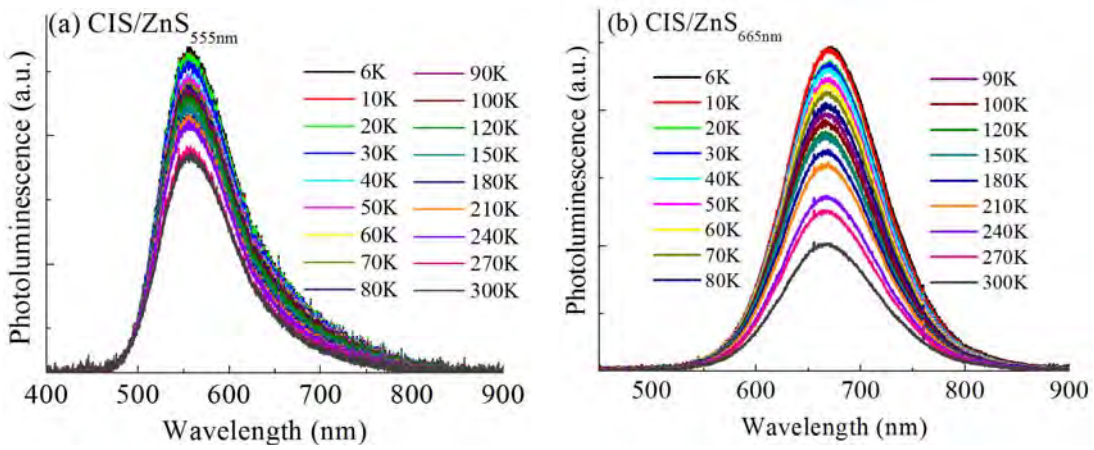

FIG. 19. Photoluminescence spectra of (a) CIS/ZnS_{555nm} and (b) CIS/ZnS_{665nm}

The PL width of CIS/ZnS_{665nm} has ~115 nm at FWHM which provides the wider spectral covering in the visible spectra for preparing white light compared to the PL width ~100 nm at FWHM from CIS/ZnS_{555nm}. However the PL from CIS/ZnS_{555nm} provides the better spectral coupling with the blue excitation for the hybrid white LEDs in the visible spectral region because CIS/ZnS_{665nm} has the undesired infrared emission from as shown in figure 20 (a). Figure 20 (b) shows the proposed schematic sketch of CIS/ZnS coreshells stacking on the InGaN blue LEDs emitting at ~470 nm. Figure 20 (c), (d), and (e) display the photo pictures of devices and emissions of InGaN (c), hybrid white LED with CIS/ZnS_{555nm} (d) and CIS/ZnS_{665nm} (e) respectively.

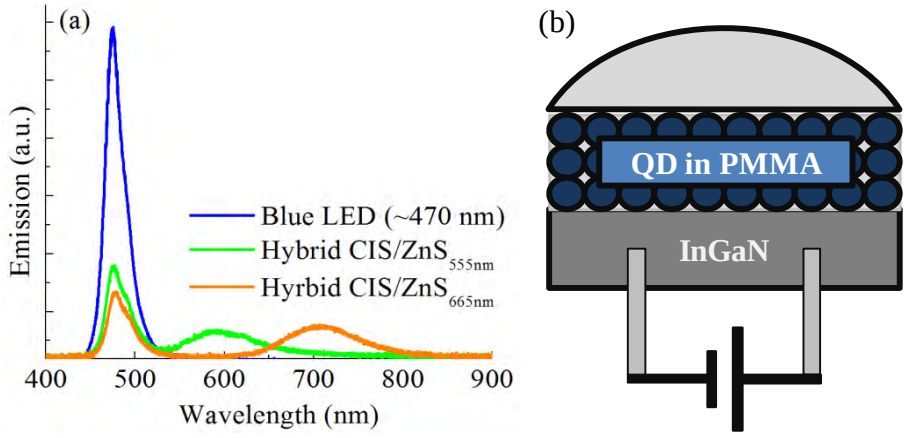

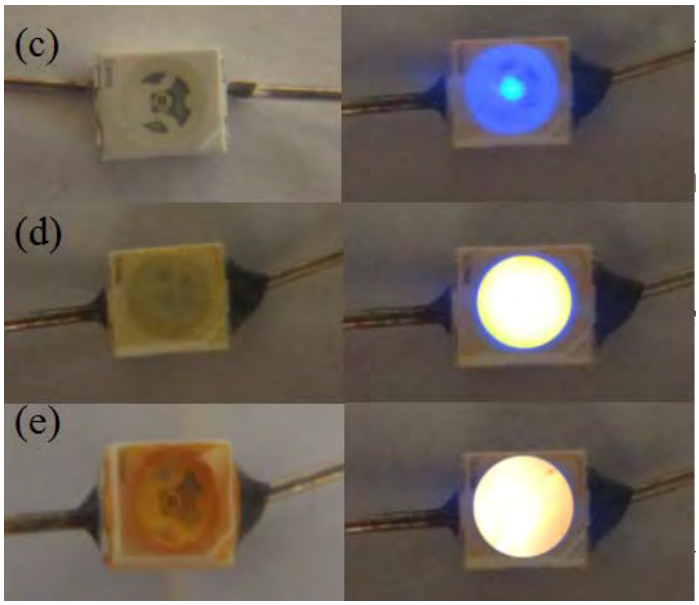

FIG. 20. (a) Emission spectra of InGaN, hybrid LED with CIS/ZnS_{555nm} and CIS/ZnS_{665nm}; (b) Proposed schematic sketch of CIS/ZnS stacking on the InGaN LED; Photo pictures of devices and emissions of (c) InGaN, (d) hybrid white LED with CIS/ZnS_{555nm} and (e) hybrid white LED with CIS/ZnS_{665nm}.

Label-free and visible quantification of glucose via an optical transduction of enzyme-mediated excitation screening and quantum dot photoluminescence irradiation

A label-free and optical biosensor is based on the irradiance changes of visible photoluminescence (PL) of quantum dots in a thin polymer film. For glucose sensing as a target molecule, the screening of UV excitation due to pre-absorption by the product of an enzymatic assay leads to the PL quenching of QDs in a non-contact scheme. The irradiance changes of QD PL indicate quantitatively the level of glucose present. The non-contact nature of bio-assay has no-surface degradation of QDs that enables efficient, waste-free, cost-effective, portable, and sustainable bio-sensor with attractive market demands. The thickness limit of detection for the non-contact QD biosensor is ~3.5 μm which is competitive with existing contact-based bioassays. In addition, the non-contact QD biosensor operates over the entire clinically relevant range of glucose concentrations of biological fluids including urine, whole blood, and etc. The comparable results with any ranges of cost-affordable detectors including spectrophotometer, portable spectrometer suggest that the label-free and visible quantification of glucose with QD film can be applied to the low-cost point-of-care biological sensing as well as scientific applications in the laboratory for characterizing glucose or other analytes.

The unique multiplexing and visual readout capabilities of optical detection provide a convenient means to assess a number of important molecules, such as glucose, which is important in public health[67], food industry[68], the life sciences[69], and etc. However, many existing techniques for optical detection of glucose suffer from low signal-to-noise (S/N) or repeatability, and have low specificity for biological fluids. The semiconductor quantum dots (QDs) for biomedical sensing are of great interest because QDs with sizes near the bulk Bohr radius exhibit good color purity,

high quantum efficiency, and large tunability in the optical spectral region[70,71,72]. In addition, the semiconductor can be incorporated into the electronic bio-device, but it can be excited electrically, for example, QD LED and the nanoscale QDs are easily integrated with flexible and portable devices. Strategies for QD-based sensing of analyte, like glucose, can be characterized by either contact or non-contact technique. The contact-based strategy refers to the director contact of QDs with the analyte-containing solution under test. Unfortunately, the contact-based strategy often modifies the solubility, aggregation behavior, surface degradation, and sensitivity of the QDs in the presence of the analyte. In addition, the direct contact-based QD sensor is limited with reusability because the QD is not easy to extract with high optical quality from the mixture solutions with various types of biomedical analytes. The contact-based bioassays using enzymatic reactions have been used to induce fluorescence quenching of QDs via irreversible degradation of the QDs,where the glucose oxidase or horseradish peroxidase leads to production of H_2O_2, and the peroxides on QD surfaces degrades the optical properties. In contrast to the destructive technique of direct contact-based bioassays, several non-contact strategies have been recently demonstrated. Therefore, the development of reusable, cost effective, portable, and user-friendly QD-based biosensor with a large dynamic range of sensitivity was an formidable challenge until this work is presented.

In this article, a noble strategy 1) An enzymatic assay produces a fluorescent product (NADH), the concentration of which is proportional to the concentration of glucose present. 2) UV light at ~365 nm is used to illuminate the solution under test, and the transmitted intensity of the UV, which is proportional to the concentration of NADH, is used to excite CdSe/ZnS core/shells. The photoluminescence (PL) irradiance of the QDs is proportional to the illumination intensity within the excitation linearity region. The excitation intensity to the QD is proportional to the transmitted intensity after the absorption of NADH. Therefore, the photoluminescence irradiance of QDs indicates the level of concentration of glucose indirectly. 3) A photo-detector in visible spectral region quantifies the PL irradiance of quantum dots and reveals the concentration level of glucose in solutions including biological fluids of blood and urine. The physical mechanism of label-free and visible biosensor is an optical transduction through optical illumination, excitation screening by biological analyte, and QD PL irradiance quenching that indicates concentration level, specifically glucose for this demonstration.

The non-contact optical transduction has several advantages over existing methods: 1) It does not require labels – the QDs intrinsically produce a visible PL upon excitation. 2) The method is non-contact because it does not require mixing the QDs with the solution under test, which saves on the cost of materials (QDs). 3) The fabricated optical transduction biosensor is reusable and waste-free because the prepared CdSe/ZnS in polymer films are photostable within the excitation illumination level, engendering the system with a long performance lifetime. 4) Once the sensors are made, sample preparation is minimal, and the sensor can work with raw biological fluids of urine and blood without additional processing. 5) Specificity of the method arises from the use of an enzymatic assay, suggesting that the strategy can be generally extended to work for other analytes besides glucose. 6) The method is general enough to be implemented with any types of compositional QDs with various morphologies. 7) The method can be implemented with low-cost detectors such as mobile phone cameras for point-of-care applications.

The optical transduction strategy of excitation screening and PL quenching was applied for the glucose concentration measurement. The optical transduction strategy is highly generalizable, and can be applied to numerous assays. While absorption-based strategies are not specific, the

specificity of such tests can be implemented through the use of enzymatic assays as the standard for most electrochemical methods is currently used[73]. This article presented a noble idea of non-contact and label-free biosensing via optical transduction with excitation screening by samples and PL quenching of QD films at the visible spectral region, and demonstrated the feasibility of cost effective, portable, and user-friendly devise. In conclusion, the label-free and non-contact biosensing via optical transduction of enzyme-mediated excitation screening and PL quenching of QD films were demonstrated as a viable strategy to measure the concentration of glucose in the visible spectral region with low-cost and point-of-care biosensing as well as scientific applications.

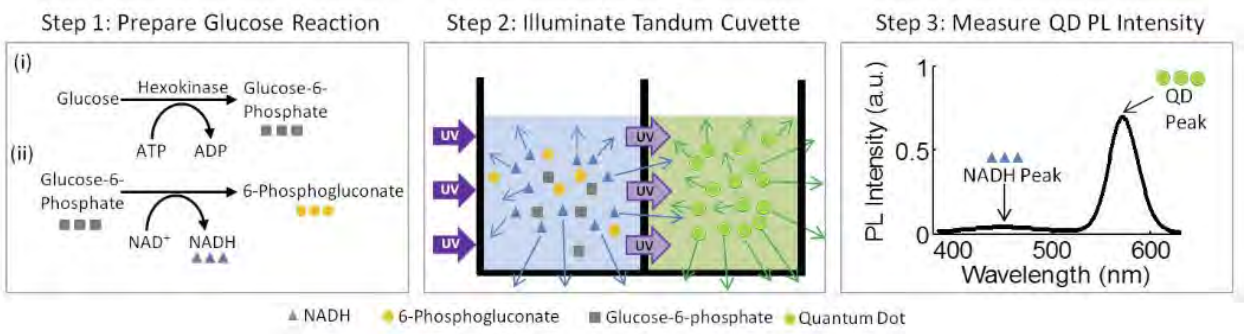

Figure 21. Schematic illustration of a non-contact optical transduction for the quantitation of glucose. The fluorescent by-product (NADH) of a hexokinase-glucose 6-phosphate dehydrogenase enzymatic glucose assay absorbs UV excitation light, leading to increased NADH fluorescence and reduced QD PL compared to when no glucose is present. The concentration of glucose present is a direct function of the QD PL, which occurs in the visible range. Residual NADH PL does not interfere with the measurement.

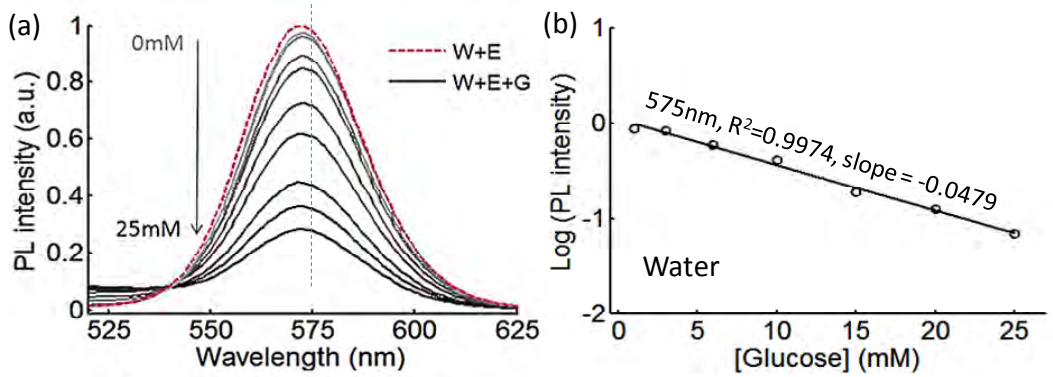

Figure 22. (a) Normalized 575-nm QD PL intensity curves for various concentrations of glucose (3.5μM, 4μM, 1mM, 3mM, 6mM, 10mM, 15mM, 20mM, 25mM). (b) Calibration curves for 575-nm QDs at a 1:100 dilution. The curve relate the measured PL intensity to the glucose concentration and are linear when plotted on a log-linear scale. All data is normalized to the PL intensity of a solution containing only water and enzymes (no glucose).

Instrumentation of Streak Camera

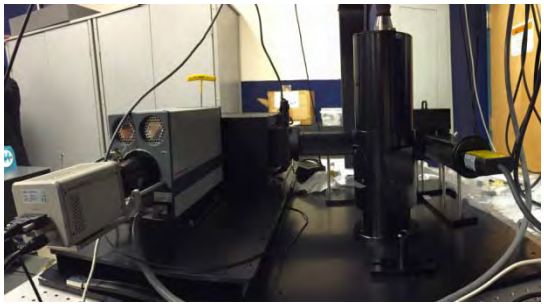


Recently the Picosecond Fluorescence Lifetime Measurement System C11200 or streak camera was acquired from Hamamatsu Photonics. Basic capabilities include measurement and analysis of temporal characteristics of fluorescent emission in a wide range of spectral regions. The streak camera uses a picosecond light pulser equipped with a temperature controlled laser diode at 405 nm with a peak power between 10 mW to 100 mW. The ultrafast optical detector, C10627 Streakscope, allows this system to capture very weak luminescence from picoseconds to milliseconds with a very high signal to noise ratio which is ideal for time-resolved spectroscopy.

The streak camera has been used to capture emission spectra and lifetimes of chalcopyrite semiconductor quantum dots as well chalcogenide materials. The dual functionality of the streak camera has permitted the study of lifetime decays and overall luminescence for characterization and analysis of several materials of high interest in the field of nanophotonics. Below are the emission spectrum and lifetime decay as well as CCD imaging of a particular sample of CdSe quantum dots with emission peak at ~532 nm.

The streak camera has also been a vital part of outreach and mentorship between local high schools in the Hampton Roads area as well as undergraduate STEM majors (Tia Westmoreland (physics); Kyle Burney (physics)). Through training and mentorship from graduate students and post-doctoral researchers, many chemistry, biology, and physics majors have benefitted from this technology. Students are trained on instrumentation and data analysis techniques with emphasis on the physical origins and meaning behind data acquired from the streak camera. The successful implementation of the streak camera promoted healthy scientific research and valuable experience for many students.

Educational Impact

Student Research Experience On-Campus:

The graduate and undergraduate students in physics, chemistry, and engineering participated in various research activities including materials preparation, microscopy samples, absorption spectroscopy, femto-second laser spectroscopy, Raman spectropy, etc. The students studied optical properties of semiconductor quantum dots, Purcell enhancement, optical flocculation, surface-enhanced Raman spectroscopy, and LED development. Their scientific findings and results were disseminated through journal articles and conference presentations. Their undergraduate capstone and graduate theses also included the experiment results and analyses

Student Research Experience Off-campus:

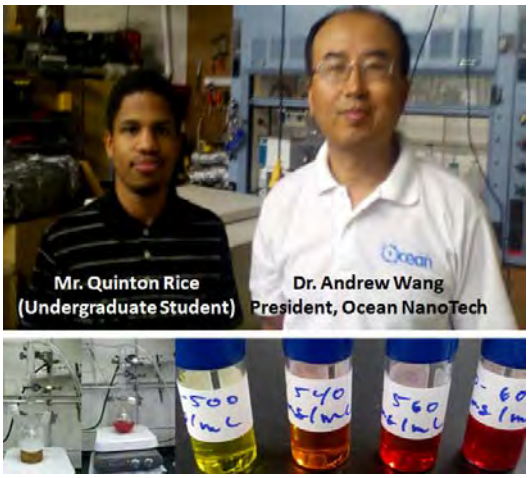

Mr. Quinton Rice (undergraduate student) visited Ocean NanoTech on August 16-18, 2012, and was trained in synthesizing quantum dots. He prepared research samples of semiconductor QDs for his undergraduate capstone thesis. He graduated from physics in May 2013, and joined my research group as a graduate student.

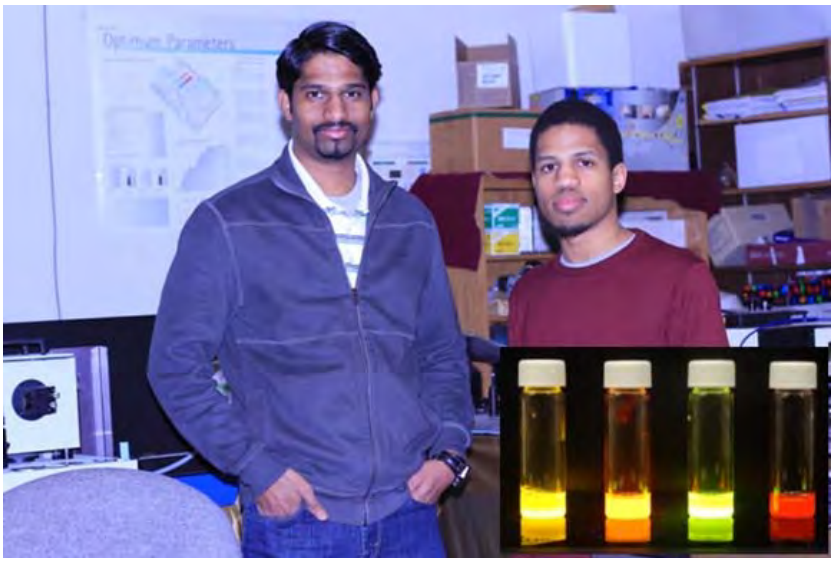

Mr. Quinton Rice (Graduate Student in Physics) visited University of North Texas and Texas Christian University on February 7-10, and April 27-May 01 for characterizing semiconductor quantum dots. Dr. Seo's group is collaborating with the scientists in the Center for Fluorescence Technologies and Nanomedicine, Department of Cell Biology and Immunology, Health Science Center University of North Texas; and Department of Physics, Texas Christian University.

Best Student Presentation Award:

Mr. Quinton Rice attended the 92nd Annual Meeting of the Virginia Academy of Science in Richmond, Virginia on May 14th through May 16th 2014 at Virginia Commonwealth University. He presented on "Temperature- and time-resolved spectroscopy of $CuInS_2$ semiconductor nanocrystals with ZnS capping" in the Astronomy, Math, and Physics with Material Science Section with Thomas C. Mosca III presiding as Chair. Mr. Rice was awarded 1st place in the oral presentation competition for Best Student Paper Presentation.

Student Graduations:

Mr. Roopchan Ramdon in physics completed his M.S. degree in fall 2012. His thesis title for M.S. degree was "Plasmon-coupled CdSe/ZnS Quantum Dots for Photonic Applications". He joined the Ph.D. program, and is working on "Theoretical studies of spin-photon entangled complementarity". Mr. Anderson Hayes in physics finished B.S. degree in May 2013 with a capstone thesis entitled "Raman spectroscopy of nicotine, quinine, and caffeine: determining the effectiveness of SERS with Au nanoparticles". He joined M.S. degree program in summer 2013, and is working on SERS and single photon spectroscopy. Mr. Quinton Rice in physics completed B.S. degree in May 2013 with a capstone thesis entitled "Temperature-Dependent Photoluminescence of CdSe Quantum Dots in Toluene". He joined the graduate program in summer 2013. He is working on "Semiconductor quantum dots and photon entanglement". Mr. Quinn Allen Hailes, undergraduate student in physics completed B.S. degree in spring 2014. His capstone thesis was "Temperature Dependent Photoluminescence of $CuInS_2$ with ZnS Capping". Quinn Allen Hailes joined the physics graduate program at Hampton University in September 2014.

Successful Transitions from Undergraduate to Graduate Studies:

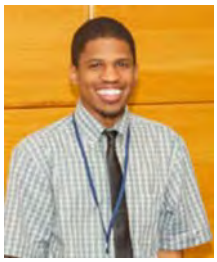

Since Mr. Quinton Rice joined the ARO program at Hampton University in 2011 as an undergraduate, he learned the essential skills to conduct high quality research while unveiling an undiscovered interest in nanoscience. Upon graduating with a Bachelor of Science in Physics, Mr. Rice joined the Master's Degree program offered at the Hampton University Graduate College. With the support of many collaborators and excellent advisement, Mr. Rice attended several important scientific conferences to disseminate the research he was conducting on semiconductor quantum dots and there practical applications. Mr. Rice excelled in the coursework while gaining more experience in the laboratory which led to his acceptance into the Ph. D. program at Hampton University. Mr. Rice has continued to excel and conduct quality research with funding from the Army Research Office. Without funding scientific research

comes to a halt, regardless of how passionate students may be. Mr. Rice is very grateful for ARO project which have contributed a great deal to his career development and overall success.

Mr. Anderson Hayes is a second-year Ph.D. student in physics, with a concentration in optics at Hampton University. Mr. Hayes joined the ARO program at Hampton University in 2012 as an undergraduate student, and excelled in the Master's program which then prompted him to transition into a Ph.D program. Currently, he is conducting research colorimetric flocculation and examining the alteration of the vibration modes of plasmonic nanoparticles. Mr. Hayes is mentoring local high school students in the Hampton Roads area on quantum dots and plasmonic nanoparticles research. Mr. Hayes has been afforded the opportunity to travel and present his research at various international and national conferences. The Army Research Office has supported Mr. Hayes' research activities throughout his tenor at Hampton University.

Summer Research Experience for Undergraduate Students in 2011:

The PI is also involved in the research experience for undergraduate students (REU) program. The selected undergraduate students in nationwide acquired excellent research experience in optical, nuclear, and medical physics, and presented their summer research activities at the end of program.

High-School Student Research and Awards:

Mr. Anderson Hayes, Physics Senior in the academic yr 2012-13, mentored a high school student Ms. Rahda Venkatesan, Junior, Grafton High School and Governor's School. Ms. Venkatesan's research project was "Molecule-linked Plasmonic Au Nanoparticles for Surface-Enhanced Raman Spectroscopy".

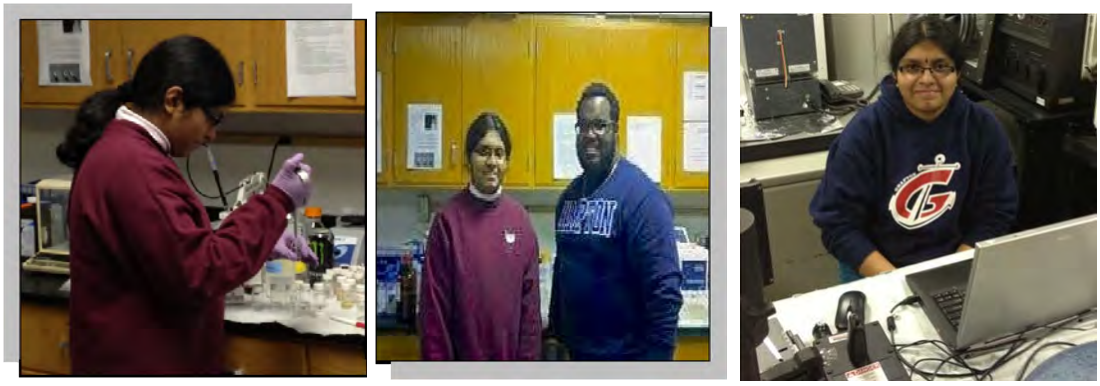

Ms. Radha Venkatesan presented her research results at the 62nd Tidewater Science Fair Competition, and received 1st place award in Materials and Bio-engineering category. Her presentation title was "Surface-Enhanced Raman Scattering for Quinine-linked Gold Nanoparticles". Tidewater Regional Science and Engineering Fair was held at Old Dominion University, Norfolk, Virginia on March 16, 2013. The Tidewater Science and Engineering Fair is open to all home-schooled, private school, and public school students from seven counties (Accomack, Gloucester, Isle of Wight, James City, Northampton, Southampton, and York) and ten cities (Chesapeake, Franklin, Hampton, Newport News, Norfolk, Poquoson, Portsmouth, Suffolk, Virginia Beach and Williamsburg) from Williamsburg to Virginia Beach.

Ms. Radha Venkatesan also participated in the Virginia State Science & Engineering Fair on April 5-6, 2013 at the Virginia Military Institute, Lexington, VA. The Virginia State Science Fair was affiliated with the International Science and Engineering Fair. High school students from across the state competed within thirteen categories. The grand prize winner was proceeded to participate in the Intel International Science and Engineering Fair. At the State Science Fair, Ms. Venkatesan received two special awards for the project. One was from SAIC for Applied Sciences. The other one was the Yale Science and Engineering Award presented by Yale

University for the Most Outstanding 11th grade Exhibit Overall from the categories of Computer Science, Engineering, Physics or Chemistry.

Recently, she was admitted to the physics program at the University of Richmond with the Presidential Scholarship $60,000, and is chosen to be a Richmond Science Scholar with Robins Science Scholar designation with $229,880.

High School Students' Summer Research Activities:

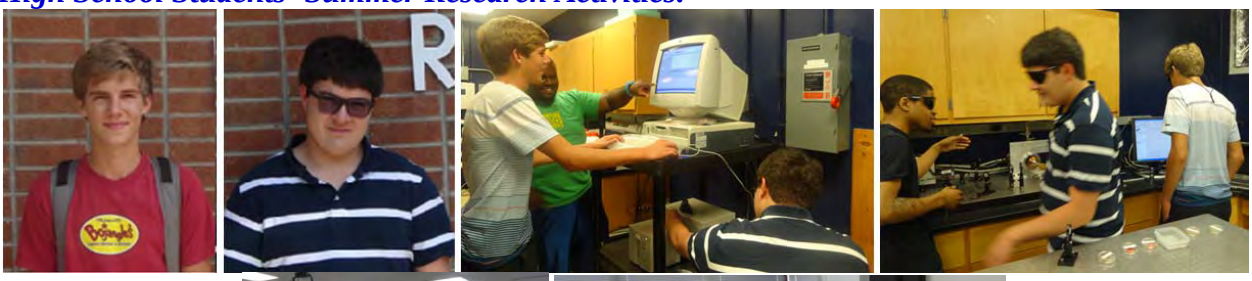

Two high school students participated in research during the summer of 2014. The high school students were Mr. James Crawford (rising Junior, Poquoson High School, Poquoson, VA) and Mr. Ryan Kilduff (rising Junior, King's Fork High School, Suffolk, VA). Dr. Bagher Tabibi provided them lectures every morning, and advised their research activities. Mr. Quinton Rice mentored Mr. James Crawford on the research project of Spectroscopic Emission Studies of

CdSe/ZnS Quantum Dots while Mr. Anderson Hayes mentored Mr. Ryan Kilduff on the research project of Absorption and Emission Properties of Gold Nanoparticles.

Hands-on Science Experience for Middle School Students:

Spratley Gifted Center requested campus visit to have them perform hands-on activities in one of five STEM laboratories – Physics, Mathematics, Computer Science, Chemistry and Atmospheric Sciences. Every department provided their best resources to engage in, stimulate and challenge the students. Mr. Roopchan Ramdon and Ms. Ashley Jackson actively involved in middle school students' hands-on experience in optical science.

High School Science Class:

Dr. Mahmoud AbdelFattah, Mr. Quinton Rice, and Mr. Anderson Hayes visited high school science classrooms, and presented 2 science-oriented talks concerning the types of energy, spectroscopy, and laser science. They also demonstrated physics concepts through the use of macroscopic gyroscopes, hoverboards, wave simulators, fiber optics, and spectrometers. The majority of students learned the topics offered. It was a great learning experience for everyone.

Physics Demonstration at Lake Taylor Middle School:

The ACLaSS Students, Mr. Quinton Rice (Graduate Student in Physics) and Mr. Anderson Hayes (Graduate Student in Physics) visited Ms. Ramos' 7th grade science class at Lake Taylor Middle School on Feburary 27, 2013 to teach the students basic physics concepts in a fun exciting way. The science teacher Ms. Elaine and our graduate students provided the middle school students' hands-on experience on the "Bicycle Wheel Gyroscope" and "Hoverboard" and taught them the important conservation law of physics: the conservation of angular momentum and the turning motion, and the basic physical concepts of air pressure, friction, and torque.

Career Fair at the Lake Taylor Middle School:

Dr. Mahmoud Abdel-Fattah, Ms. LeAnna Austin, Mr. Quinton Rice, and Mr. Anderson Hayes visited the Lake Taylor Middle School on February 27, 2013 for their Career Fair. The participants in the project explained careers in the science to the middle school students. The participants also provided the fun demonstrations of waves and lights and explained the basic concepts of physics behind the optics.

Norview High School STEM Career Day:

The students in the project, Mr. Anderson Hayes (Graduate Student in Physics) and Mr. Quinn Hailes (Senior in Physics), attended at the Norview High School's Science, Technology, Engineering and Mathematics (STEM) Career Day on November 6, 2013. The students raised awareness of viable, and relevant, STEM career options to students from various backgrounds and skill levels. Also the ACLaSS students discussed with high school students the various research opportunities in the ACLaSS at Hampton University.

Lake Taylor Middle School in summer 2014:

Mr. Quinton Rice, Mr. Anderson Hayes, Ms. LeAnna Austin, Dr. Mahmoud Abdel-fattah, Dr. Bagher Tabibi, and Dr. Jaetae Seo visited Lake Taylor Middle School in Norfolk, Virginia on July 16, 2014 to explain the concepts of optics and fun physics. Mr. Quinton Rice and Mr. Anderson Hayes demonstrated spectroscopy of white light, spectroscopy on halogen lamps, as well as the polarization of light. Dr. Mahmoud Abdel-fattah, Dr. Bagher Tabibi, Ms. LeAnna Austin, and Dr. Jaetae Seo also assisted in demonstrating the gyroscope and hoverboard props to teach fundamental physics concepts.

Annual Optics and Laser Science Workshop for Middle and High School Teachers:

The workshop was organized in order to engage the highest level of expertise to implement optics and nanoscience in grades 6 – 12 in summer 2012. The participating science teachers were selected from forty-nine public and private high-schools in the Hampton Roads area which covers Chesapeake, Hampton, Jamestown, Newport News, Norfolk, Portsmouth, Suffolk, Virginia Beach, Williamsburg and Yorktown in the state of Virginia. The optics and laser science modules are being developed at Hampton University with the teacher participants in the first fiscal yr to implement the advanced education modules in the academic classroom next year. The education modules include wavy light, electromagnetic energy, fireworks, weather and spectroscopy, laser lesson, and color of fish in the sea.

The researchers in the project participated in the 2013 Optics and Laser Science Summer Workshop at Hampton University on June 17-21, 2013 in order to engage the highest level of expertise to implement optics and laser science in grades 6 – 12. The participating science teachers were selected from forty-nine public and private high-schools in the Hampton Roads which covers Chesapeake, Hampton, Jamestown, Newport News, Norfolk, Portsmouth, Suffolk, Virginia Beach, Williamsburg and Yorktown in the state of Virginia. The education modules for this yr include diffraction, reflection and refraction, lenses and mirrors, and emission spectra which are advanced optics topics for high school students.

The 2014 Optics and Laser Science Summer Workshop was at Hampton University on June 23-27, 2014 in order to promote the science education in grades 6 – 12. The participating science teachers were selected from forty-nine public and private high-schools in Hampton Roads which covers Chesapeake, Hampton, Jamestown, Newport News, Norfolk, Portsmouth, Suffolk, Virginia Beach, Williamsburg and Yorktown in the state of Virginia. One of the science teachers participated from Pennsylvania. The participating teachers performed four modules. The first module entitled “Polarization of Light” aimed to introduce the property of polarization of light through reflection, Brewster’s angle, and applications. The second module entitled “Reasons for Seasons” was proposed to explain the true reason for seasonal variations in temperature. This module was inspired by the fact that many people believe that the distance from the sun is the reason for seasons, this module shows, with simple supplies, that the angular tilt of the earth axis with respect to the normal to earth’s rotational plane is the true factor. The third module of “The Pretty Colors” was based on spectroscopy. Different light sources were used to analyze their spectral components using spectroscopes and spectrometers. The fourth and last module “Reflection of Light” had an interesting idea of recycling household items and using arts and crafts to build a kaleidoscope where the students experiment with the reflections of light. Four invited speakers presented to the teachers; Dr. Tarek Abdel-Fattah from Christopher Newport University (CNU) presented about his research on carbon nanotubes, Dr. Mahmoud Abdel-Fattah from Hampton University presented about the properties of light, Dr. Sainath Babu from Hampton University presented about PBA toxicology, and Dr. Wei Cao from Old Dominion University (ODU) presented about the electron microscope. The teachers enjoyed a site visit to the Hampton University Proton Therapy Institute (HUPTI) where they received a tour by the executive director Mr. Keith Gregory. It was very interesting and educational tour. Finally, the teachers gave their own presentations that included their comments and tweaks of the four modules.

Collaborative Laser and Materials Workshop:

Dr. Jaetae Seo organized "Collaborative Laser and Materials Workshop," on February 6, Thursday, 2014 in order to prepare electric materials for brain research using ultrafast lasers between Norfolk State University and Hampton University. The participants from NSU were Dr. Patricia F. Mead, Dr. Kyo D. Song, and Mr. William Harkins. The faculties and students at both institutions presented and discussed their research activities, and discussed collaborative activities. Dr. Calvin Lowe (Dean, School of Science) supported for the successful workshop.

Curriculum Development:

Dr. Jaetae Seo, Dr. Bagher Tabibi, and Dr. Mahmoud Abdel-Fattah offered two advanced courses of PHY723 Quantum Nonlinear Optics and PHY728 Quantum Electrodynamics to provide the ACLaSS students with theoretical and experimental curricula that could support them to carry out their research as well as to assist the proposed research activities. Four graduate students attended the classes, and learned the fundamental concepts and current trends of quantum optics and quantum nonlinear optics research. Also the students involved in the hands-on experience in the laboratory in the selected research topics.

List of Impacts on Research Grant Award and Program Developments:

- Grant Award from National Science Foundation
  Title: Advanced Center for Laser Science and Spectroscopy
  Program Director and P.I.: Jaetae Seo

Amount: $5,000,000; Time Period: September 01, 2011 – August 31, 2016

- Grant Agency: National Science Foundation (in preparation)
  Program: Emerging Frontiers in Research and Innovation 2015
  Title: Quantum Coherence in Atomic Layer (QCAL)
  PI: Felix Jaetae Seo with Co-PI: Audrey Ellerbee (Stanford University) and Helmut Baumgart (Old Dominion University)
  Amount: $2,000,000; Time Period: October 01, 2015 – September 30, 2019

- Grant Agency: National Aeronautics and Space Administration (NASA) (in preparation)
  Title: HU Center for Atmospheric Research and Education
  PI: William Moore; Amount: $5,000,000
  Sub-Title: Nonlinear Classical and Quantum Photons for Advanced Lidar
  Co-I: Felix Jaetae Seo; Amount: $762,500
  Time period: May 2015 – September 2020

Bibliography

[1] (a) J. A. Smyder, T. D. Krauss, "Coming attraction for semiconductor quantum dots," Materials Today 14, 382 (2011); (b) Q. Dai, C. E. Duty, and M. Z. Hu, "Semiconductor-Nanocrystals-Based White Light-Emitting Diodes," Small 6, 1577 (2010); (c) Y. Zhang and A. Clapp, "Overview of Stabilizing Ligands for Biocompatible Quantum Dot Nanocrystals," Sensors 11, 11036 (2011); and (d) G. Zhang , S. Finefrock , D. Liang, G. G. Yadav, H. Yang, H. Fang, and Y. Wu, "Semiconductor nanostructure-based photovoltaic solar cells," Nanoscale 3, 2430 (2011).

[2] (a) S. M. Ma, J. T. Seo, Q. Yang, R. Battle, L. Creekmore, K. Lee, B. Tabibi, and W. Yu, "The Second Hyperpolarizability of CdTe Nanocrystals using Polarization-resolved Degenerate Four-Wave Mixing," Applied Surface Science 253, 6612 (2007); (b) Q. Dai, Y. Wang, X. Li, D. J. Pellegrino, Y. Zhang, M. Zhao, B. Zou, J.T. Seo, Y. Wang, and W. W. Yu, "Size-dependent Composition and Molar Extinction Coefficient of PbSe Semiconductor Nanocrystals," American Chemical Society-Nano 3(6), 1518 (2009).

[3] L. Qu and X. Peng, "Control of Photoluminescence Properties of CdSe Nanocrystals in Growth," J. Am. Chem. Soc. 124, 2049 (2002).

[4] A. A. Chistyakov, I. L. Martynov, K. E. Mochalov, V. A. Oleinikov, S. V. Sizova, E. A. Ustinovich, and K. V. Zakharchenko, "Interaction of CdSe/ZnS core-shell semiconductor nanocrystals in solid thin films," Laser Phys. 16, 1625 (2006).

[5] R. R. Chance, A. Prock, and R. Silbey, "Lifetime of an emitting molecule near a partially reflecting surface," J. Chem. Phys. 60, 2744 (1974).

[6] S. F. Wuister, I. Swart, F. van Deriel, S. G. Hickey, and C. de M. Donega, "Highly Luminescent Water-Soluble CdTe Quantum Dots," Nano Letters 3(4), 503 (2003)

[7] K. Hosoki, T. Tayagaki, S. Yamamoto, K. Matsuda, and Y. Kanemitsu, "Direct and Stepwise Energy Transfer from Excitons to Plasmons in Close-Packed Metal and Semiconductor Nanoparticle Monolayer Films," Physical Review Letters 100, 207404 (2008).

[8] Y. Ito, K. Matsuda, and Y. Kanemitsu, "Mechanism of photoluminescence enhancement in single semiconductor nanocrystals on metal surfaces," Phy. Rev. B 75, 033309 (2007).

[9] A. A. Chistyakov, I. L. Martynov, K. E. Mochalov, V. A. Oleinikov, S. V. Sizova, E. A. Ustinovich, and K. V. Zakharchenko, "Interaction of CdSe/ZnS core-shell semiconductor nanocrystals in solid thin films," Laser Phys. 16, 1625 (2006).

[10] D. Ratchford, F. Shafiei, S. Kim, S. K. Gray, and X. Li, "Manipulating Coupling between a Single Semiconductor Quantum Dot and Single Gold Nanoparticle," Nano Lett. 11, 1049 (2011).

[11] (a) Maria Veronica Rigo and Jaetae Seo, "Probing Plasmon Polarization-Mediated Photoluminescence Enhancement on Metal-Semiconductor Hybrid Optical Nanostructures," Chemical Physics Letters 517, 190 (2011); and (b) H. Mertens, J. S. Biteen, H. A. Atwater, and A. Polman, "Polarization-Selective Plasmon-Enhanced Silicon Quantum-Dot Luminescence," Nano Lett. 6, 2622 (2006).

[12] W. Yu, L. Qu, W. Guo, and X. Peng, "Experimental Determination of the Extinction Coefficient of CdTe, CdSe, and CdS Nanocrystals," Chem. Mater. 15, 2854 (2003).

[13] Jaetae Seo, Rafal Fudala, Wan-Joong Kim, Ryan Rich, Bagher Tabibi, Hyoyeong Cho, Zygmunt Gryczynski, Ignacy Gryczynski, and William Yu, "Hybrid Optical Materials of Plasmon-coupled CdSe/ZnS Coreshells for Photonic Applications," Optical Materials Express 2, 1026 (2012).

[14] Woo-Seuk Song and Heesun Yang, "Fabrication of white light-emitting diodes based on solvothermally synthesized copper indium sulfide quantum dots as color converters," Applied Physics Letters 100, 183104 (2012).

[15] Yu Zhang, Chuang Xie, Huaipeng Su, Jie Liu, Shawn Pickering, Yongqiang Wang, William W. Yu, Jingkang Wang, Yiding Wang, Jong-in Hahm, Nicholas Dellas, Suzanne E. Mohney, and Jian Xu, "Employing Heavy Metal-Free Colloidal Quantum Dots in Solution-Processed White Light-Emitting Diodes," Nano Lett. 11, 329 (2011).

[16] Dawei Deng, Yuqi Chen, Jie Cao, Junmei Tian, Zhiyu Qian, Samuel Achilefu, and Yueqing Gu, "High-Quality CuInS2/ZnS Quantum Dots for In vitro and In vivo Bioimaging," Chemistry of Materials 24, 3029 (2012).

[17] Elsa Cassette, Marion Helle, Lina Bezdetnaya, Frédéric Marchal, Benoit Dubertret, Thomas Pons, "Design of new quantum dot materials for deep tissue infrared imaging," Advanced Drug Delivery Reviews, in press.

[18] W. W. Yu, and X. Peng, "Formation of high-quality CdS and other II-VI semiconductor nanocrystals in noncoordinating solvents: Tunable reactivity of monomers," Angew. Chem. Int. Ed. 41, 2368 (2002).

[19] Quanqin Dai, Yingnan Wang, Ruowang Li, Yu Zhang, Xinbi Li, Ruowang Li, Bo Zou, Jaetae Seo, Yiding Wang, Manhong Liu, and William W. Yu "Stability study of PbSe Semiconductor Nanocrystals over Concentration, Size, Atmosphere, and Light Exposure" Langmuir *25* (20), 12320 (2009).

[20] Renguo Xie, David Battaglia, and Xiaogang Peng, "Colloidal InP Nanocrystals as Efficient Emitters Covering Blue to Near-Infrared," J. Am. Chem. Soc. 129, 15432 (2007).

[21] Shu Xu, Jan Ziegler and Thomas Nann, "Rapid synthesis of highly luminescent InP and InP/ZnS nanocrystals," J. Mater. Chem.18, 2653 (2008).

[22] Shuai Gao, Chunfeng Zhang, Yanjun Liu, Huaipeng Su, Lai Wei, Tony Huang, Nicholas Dellas, Shuzhen Shang, Suzanne E. Mohney, Jingkang Wang, and Jian Xu, "Lasing from colloidal InP/ZnS quantum dots," Optics Express 19, 5528 (2011).

[23] W. W. Yu, Y. A. Wang, and X. Peng, "Formation and stability of size-, shape-, and structure-controlled CdTe nanocrystals: ligand effects on monomers and nanocrystals," Chem. Mater. 15, 4300 (2003).

[24] L. Li, T. J. Daou, I. Texier, T. T. K. Chi, N. Q. Liem, and P. Reiss, "Highly luminescent CuInS2/ZnS core/shell nanocrystals: cadmium-free quantum dots for in vivo imaging", Chem. Mater. 21, 2422 (2009).

[25] H. Zhong, Y. Zhou, M. Ye, Y. He, J. Ye, C. He, C. Yang, and Y. Li, "Controlled synthesis and optical properties of colloidal ternary chalcogenide CuInS2 nanocrystals", Chem. Mater. 20, 6434 (2008).

[26] C. Xie, Y. Zhang, A. Y. Wang, W. W. Yu, J. Wang, and J. Xu, "Stability investigation of CuInS2-based heavy-metal free nanocrystals," MRS Proc. 1316, QQ3.3 (2011).

[27] Wenjin Zhang and Xinhua Zhong, "Facile Synthesis of ZnS_CuInS2-Alloyed Nanocrystals for a Color-Tunable Fluorchrome and Photocatalyst," Inorg. Chem. 50, 4065 (2011).

[28] Luca De Trizio, Mirko Prato, Alessandro Genovese, Alberto Casu, Mauro Povia, Roberto Simonutti, Marcelo J. P. Alcocer, Cosimo D'Andrea, Francesco Tassone, and Liberato Manna, "Strongly

Fluorescent Quaternary Cu−In−Zn−S Nanocrystals Prepared from $Cu_{1-x}InS2$ Nanocrystals by Partial Cation Exchange," Chem. Mater. 24, 2400 (2012).
[29] H. Nakamura, W. Kato, M. Uehara, K. Nose, T. Omata, S. Otsuka-Yao-Matsuo, M. Miyazaki, and H. Maeda, "Tunable photoluminescence wavelength of chalcopyrite CuInS2-based semiconductor nanocrystals synthesized in a colloidal system", Chem. Mater. 18, 3330 (2006).
[30] Masato Uehara, Kosuke Watanabe, Yasuyuki Tajiri, Hiroyuki Nakamura, and Hideaki Maeda, "Synthesis of $CuInS_2$ fluorescent nanocrystals and enhancement of fluorescence by controlling crystal defect," The Journal of Chemical Physics 129, 134709 (2008).
[31] Ching-Hwa Ho, "Temperature Dependent Crystal-Field Splitting and Band-Edge Characteristic in $Cu(Al_xIn_{1-x})S_2$ Series Solar Energy Materials," J. Electrochem. Soc. 158, H554 (2011).
[32] Young-Kuk Kim, Si-Hyun Ahn, Gyu-Chae Choi, Kookchae Chung, Young-Sang Cho, and Chul-Jin Choi, "Photoluminescence of CuInS2/(Cd,Zn)S Nanocrystals as a Function of Shell Composition," Transcations on Electrical and Electronic Materials 12, 218 (2011).
[33] Andrew M. Smith, Aaron M. Mohs and Shuming Nie, "Tuning the optical and electronic properties of colloidal nanocrystals by lattice strain," Nature Nanotechnology 4, 56 (2009).
[34] Hideyuki Maki, Testuya Sato, and Koji Ishibashi, "Direct Observation of the Deformation and the Band Gap Change from an Individual Single-Walled Carbon Nanotube under Uniaxial Strain," Nano Letters 7, 890 (2007).
[35] Yong-Hua Li, X. G. Gong, and Su-Huai Wei, "*Ab initio* all-electron calculation of absolute volume deformation potentials of IV-IV, III-V, and II-VI semiconductors: The chemical trends," Physical Review B 73, 245206 (2006).
[36] J. Persson, U. Hakanson, M. K.-J. Johansson, L. Samuelson, and M.-E. Pistol, "Strain effects on individual quantum dots: Dependence of cap layer thickness," Physical Review B 72, 085302 (2005).
[37] L. Li, A. Pandey, D. J. Werder, B. P. Khanal, J. M. Pietryga and V. I. Klimov, "Efficient Synthesis of Highly Luminescent Copper Indium Sulfide-Based Core/Shell Nanocrystals with Surprisingly Long-Lived Emission," J. Am. Chem. Soc. 133, 1176 (2011).
[38] J. Park and S. W. Kim, **"**$CuInS_2$/ZnS core/shell quantum dots by cation exchange and their blue-shifted photoluminescence**,"** J. Mater. Chem. 21, 3745 (2011).
[39] Xinhua Zhong, Mingyong Han, Zhili Dong, Timothy J. White, and Wolfgang Knoll, "Composition-Tunable ZnxCd1-xSe Nanocrystals with High Luminescence and Stability," J. Am. Chem. Soc. 125, 8589 (2003).
[40] Young-Kuk Kim, Young-Sang Cho, Kookchae Chung, Chul-Jin Choi, and Pyung-Woo Shin, "Enhanced Luminescence of Cu–In–S Nanocrystals by Surface Modification," J. Nanosci. Nanotechnol. 12, 1 (2012).
[41] Stephanie L. Castro, Sheila G. Bailey, Ryne P. Raffaelle, Kulbinder K. Banger, and Aloysius F. Hepp, "Synthesis and Characterization of Colloidal CuInS2 Nanoparticles from a Molecular Single-Source Precursor," J. Phys. Chem. B 108, 12429 (2004).
[42] Vamsi K. Komarala, Chuang Xie, Yongqiang Wang, Jian Xu, and Min Xiao, "Time-resolved photoluminescence properties of $CuInS_2$/ZnS nanocrystals: Influence of intrinsic defects and external impurities," Journal of Applied Physics 111, 124314 (2012).
[43] H. Y. Ueng and H. L. Hwang, "The defect structure of $CuInS_2$. part I: Intrinsic defects," J. Phys. Chem. Solids 50, 1297 (1989).
[44] Y. Hamanaka, T. Kuzuya, T. Sofue, T. Kino, K. Ito, K. Sumiyama, "Defect-induced photoluminescence and third-order nonlinear optical response of chemically synthesized chalcopyrite $CuInS_2$ nanoparticles," Chemical Physics Letters 466, 176 (2008).
[45] Katsuhiro Nose, Yuki Soma, Takahisa Omata, and Shinya Otsuka-Yao-Matsuo, "Synthesis of Ternary CuInS2 Nanocrystals; Phase Determination by Complex Ligand Species,"Chem. Mater. 21, 2607 (2009).
[46] T. Enzenhofer, T. Unold, R. Scheer, and H. W. Schock, " Effect of Zn and Mg doping on CuInS thin films and solar cells," Mater. Res. Symp. Proc. 865, F11.3.1 (2005).

[47] H. Shibata, "Negative Thermal Quenching Curves in Photoluminescence of Solids," Jpn. J. Appl. Phys. 37, 550 (1998).

[48] Woo-Seuk Song, Sun-Hyoung Lee, and Heesun Yang, "Fabrication of warm, high CRI white LED using non-cadmium quantum dots," Optical Materials Express 3, 1468 (2013).

[49] Woo-Suek Song and Heesun Yang. "Fabrication of white light-emitting diodes based on solvothermally synthesized copper indium sulfide quantum dots as color converters", Appl. Phys. Lett. 100, 183104 (2012).

[50] Yu Zhang, Chuang Xie, Huaipeng Su, Jie Liu, Shawn Pickering, Yongqiang Wang, William W. Yu, Jingkang Wang, Yiding Wang, Jong-in Hahm, Nicholas Dellas, Suzanne E. Mohney, and Jian Xu. "Employing Heavy Metal-Free Colloidal Quantum Dots in Solution-Processed White Light-Emitting Diodes" Nano Lett. 11, 329 (2011).

[51] Masato Uehara, Kosuke Watanabe, Yasuyuki Tajiri, Hiroyuki Nakamura and Hideaki Maeda. "Synthesis of CuInS2 fluorescent nanocrystals and enhancement of fluorescence by controlling crystal defect" J. Chem. Phys. 129, 134709 (2008).

[52] Z. Peng and Xiaogang Peng. "Formation of High-Quality CdTe, CdSe, and CdS Nanocrystals Using Cd O as Precursor" J. Am. Chem. Soc. 123, 183-184 (2001).

[53] David R. Baker and Prashant V. Kamat. "Tuning the Emission of CdSe Quantum Dots by Controlled Trap Enhancement" Langmuir 26(13), 11272–11276 (2010).

[54] Haizheng Zhong, Yi Zhou, Mingfu Ye, Youjun He, Jianping Ye, Chang He, Chunhe Yang and Yongfang Li. "Controlled Synthesis and Optical Properties of Colloidal Ternary Chalcogenide CuInS2 Nanocrystals" Chem. Mater. 20, 6434–6443 (2008).

[55] Y. Hamanaka, T. Kuzuya, T. Sofue, T. Kino, K. Ito, and K. Sumiyama. "Defect-induced photoluminescence and third-order nonlinear optical response of chemically synthesized chalcopyrite CuInS2 nanoparticles" Chem. Phys. Lett. 466 (4-6), 176-180 (2008).

[56] Stephanie Castro, Sheila Bailey, Ryne Raffaelle, Kulbinder Banger, and Aloysius Hepp. "Synthesis and Characterization of Colloidal CuInS2 Nanoparticles from a Molecular Single-Source Precursor" J. Phys. Chem. B 108 (33), 12429-2435 (2004).

[57] Herng Yi Ueng and Huey-Liang. Hwang. "The defect structure of CuInS2. part I: Intrinsic efects" J. Phys. Chem. Sol. 50 (12), 1297-305 (1989).

[58] Vamsi K. Komarala, Chuang Xie, Yongqiang Wang, Jian Xu, and Min Xiao. "Time-resolved photoluminescence properties of CuInS2/ZnS nanocrystals: Influence of intrinsic defects and external impurities" J. Appl. Phys. 111, 124314 (2012).

[59] Jaetae Seo, Sangram Raut, Mahmoud Abdel-Fattah, Quinton Rice, Bagher Tabibi, Ryan Rich, Rafal Fudala, Ignacy Gryczynski, Zygmunt Gryczynski, Wan-Joong Kim, Sungsoo Jung, and Ruh Hyun. "Time-resolved and temperature-dependent photoluminescence of ternary and quaternary nanocrystals of CuInS2 with ZnS capping and cation exchange" J. App.Phys. 114 (9), 094310 (2013).

[60] Young-Kuk Kim, Si-Hyun Ahn, Kookchae Chung, Young-Sang Cho, and Chul-Jin Choi. "The photoluminescence of CuInS2 nanocrystals: effect of non-stoichiometry and surface modification" J. Mater. Chem. 22 (4), 1516 (2011).

[61] S. Neeleshwar, C. L. Chen, C. B. Tsai, Y. Y. Chen, C. C. Chen, S. G. Shyu, and M. S. Seehra. "Size-dependent properties of CdSe quantum dots" Phys. Rev. B 71, 201307 (2005).

[62] Wonkeun Chung, Hyunchul Jung, Chang Hun Lee, Sun Hee Park, Jihyun Kim, and Sung Hyun Kim. "Synthesis and Application of Non-Toxic ZnCuInS2/ZnS Nanocrystals for White LED by Hybridization with Conjugated Polymer" J. Electrochem. Soc. 158(12), H1218 (2011).

[63] Liang Li, T. Jean Daou, Isabelle Texier, Tran Thi Kim Chi, Nguyen Quang Liem, and Peter Reiss "Highly Luminescent CuInS2/ZnS Core/Shell Nanocrystals: Cadmium-Free Quantum Dots for In Vivo Imaging" Chem. Mater. 21 (12), 2422-2429 (2009).

[64] Hyunki Kim, Ji Yeon Han, Dong Seok Kang, Sung Wook Kim, Dong Seon Jang, Minwon Suh, Artavazd Kirakosyan, Duk Young Jeon. "Characteristics of CuInS2/ZnS quantum dots and its application on LED" J. Crys. Gro. 326, 90-93 (2011).

[65] Peter Reiss, Myriam Protie`re, and Liang Li. “Core/Shell Semiconductor Nanocrystals” Small 5(2), 154–168 (2009).

[66] Young-Kuk Kim and Chul-Jin Choi. “Tailoring the Morphology and the Optical Properties of Semiconductor Nanocrystals by Alloying” Nanocrystal, Dr. Yoshitake Masuda (Ed.), ISBN: 978-953-307-199-2 (2011).

[67] American Diabetes Association, “Executive summary: standards of medical care in diabetes-2011,” Diabetes Care 34, Supplemental 1, S4–10 (2011).

[68] L. A. Terry, S. F. White, and L. J. Tigwell, "The application of biosensors to fresh produce and the wider food industry," J. Agric. Food Chem. 53, 1309 (2005).

[69] D. M. Porterfield, "Measuring metabolism and biophysical flux in the tissue, cellular and sub-cellular domains: recent developments in self-referencing amperometry for physiological sensing," Biosens. Bioelectron. 22, 1186 (2007).

[70] A. Magdalena Pisoschi, "Glucose Determination by Biosensors," Biochem. Anal. Biochem. 1, 1 (2012).

[71] Sanghee Kim, Jaetae Seo, Roopchan Ramdon, Hyeon-Bong Pyo, Kyuho Song, and Byoung Hun Kang, “Solid-Phase Immunoassay of Polystyrene-Encapsulated Semiconductor Coreshells for Cardiac Marker Detection,” Journal of Nanomaterials 2012, 693575 (2012).

[72] Jaetae Seo, Rafal Fudala, Wan-Joong Kim, Ryan Rich, Bagher Tabibi, Hyoyeong Cho, Zygmunt Gryczynski, Ignacy Gryczynski, and William Yu, “Hybrid Optical Materials of Plasmon-coupled CdSe/ZnS Coreshells for Photonic Applications,” Optical Materials Express 2, 1026 (2012).

[73] P. Hilditch and M. Green, "Disposable electrochemical biosensors," J. Analyst 116, 1217 (1991).